High Temperature Materials and Processes, Vol. 6,No. 3&4, 1984, 155-194

A Review of Material Response and Life Prediction Techniques under Fatigue–Creep Loading Conditions

D.A. Miller

CEGB South Western Region, Bristol, England

R.H. Priest

Berkeley Nuclear Labs, Berkeley, Gloucestershire, England

E.G. Ellison

Mechanical Engineering Dept, University of Bristol, Bristol, England

CONTENTS

	Page
ABSTRACT	156
1. INTRODUCTION	156
2. MATERIAL RESPONSE UNDER FATIGUE-CREEP CONDITIONS	156
2.1. Cycle Type and Failure Mode	156
2.2. Ferritic Steels	158
2.3. Austenitic Stainless Steels	159
2.4. Nickel Base Alloys	163
2.5. Ductility	166
2.6. Environment	168
3. LIFE PREDICTION TECHNIQUES	170
3.1. Linear Life Fraction	170
3.2. Frequency Separation	171
3.3. Strainrange Partitioning	173
3.4. Damage Rate	175
3.5. Ductility Exhaustion	176
3.6. Crack Propagation	180
4. DISCUSSION	183
4.1. Background	183
4.2. Design Codes	183
4.2.1. Inelastic route	184
4.2.2. Elastic route	185
4.3. Future Developments	185
5. CONCLUDING REMARKS	192
REFERENCES	192

ISSN 0334-1704

ABSTRACT

The response of a range of steels and nickel base alloys to simultaneous fatigue-creep deformation is reviewed. Failure modes as well as endurance data are presented, the influence of ductility being highlighted.

Several currently used life prediction techniques are critically assessed against a range of data. The two most accurate methods appear to be a damage rate approach and ductility exhaustion. The one most easily accommodated into working design codes is identified to be ductility exhaustion. The possible incorporation of this method into ASME Code Case N-47 is proposed. Potential difficulties with this, and some areas for future work, are finally discussed.

1. INTRODUCTION

During service, components operating in power generating equipment such as power stations, gas turbines, etc., are exposed to a range of loading conditions. These include cyclic plasticity, which arises as a result of start up and shut down procedures, together with the interspersion of time dependent creep effects due to 'on-load' periods at high temperatures. Power plant components therefore have to be designed not only against creep but also fatigue. In addition, the possibility of an interaction between the two mechanisms has to be considered. Further complications arise from the influence of environment and the long term microstructural stability of the engineering alloys from which these components are manufactured.

In order that the design engineer can make realistic life predictions to ensure the integrity of these components throughout their lifetime, a knowledge of how the above mechanisms interact to cause failure is required. This knowledge can then be used in the development of constitutive failure equations and design codes.

Historically, the basis of design procedures is empirical. Results obtained from short-term laboratory tests on smooth specimens were simply extrapolated (allowing for an arbitrary safety factor) to give design lifetimes under realistically low strain ranges and/or hold-time conditions. Because the deformation processes occurring in service are so complex, testing techniques which aim to simulate these processes have to be simplified. Uniaxial mechanical cycling in air, under isothermal conditions (at temperatures typical of those experienced in service), is generally used to represent actual service conditions, though more recent tests have been performed which involve simultaneous temperature and strain cycling, in an attempt to simulate service conditions more closely /1, 2/.

Crack initiation is presently identified as being the important design criterion for in-service components: the endurance of smooth laboratory test specimens is used to represent the number of cycles taken up in the crack initiation event /3/. However, it should be noted that in power plant applications small cracks may appear early on in the components' life, and withdrawal from service at this point may be unnecessary from both a safety and an economic viewpoint. Thus, a better design criterion may be one that considers crack propagation, and much work has also been performed to investigate this approach. This work has recently been reviewed by Ellison and Harper /4/, and no further discussion will be made in this paper.

Many different techniques of life prediction for components under cyclic/hold conditions are currently available; a large number of them are still empirical. However, as the demand for higher temperatures in power generating equipment increases, so, too, does the need to understand the deformation processes occurring in industrial applications, if economical and safe plant is to be designed. Thus, more recent attempts to evolve prediction techniques have been based on metallographic observation of the damage processes, enabling the correct failure mode to be established.

The aim of this review is firstly to summarise the response of various engineering materials to cyclic-creep loading, in order to identify those parameters which govern the various failure modes. A critical review of the multitude of life prediction techniques presented in the literature is then undertaken, the most promising methods being highlighted. ASME Code Case N-47 /5/ is subsequently introduced and its merits and faults discussed. Possible ways of incorporating some aspects of existing life prediction techniques into this code, in order to improve it, are then considered. Finally, the possible direction of future work within this area is discussed.

2. MATERIAL RESPONSE UNDER FATIGUE-CREEP CONDITIONS

2.1. Cycle Type and Failure Mode

The different waveforms most frequently used during fatigue-creep testing are shown in Fig. 1. A

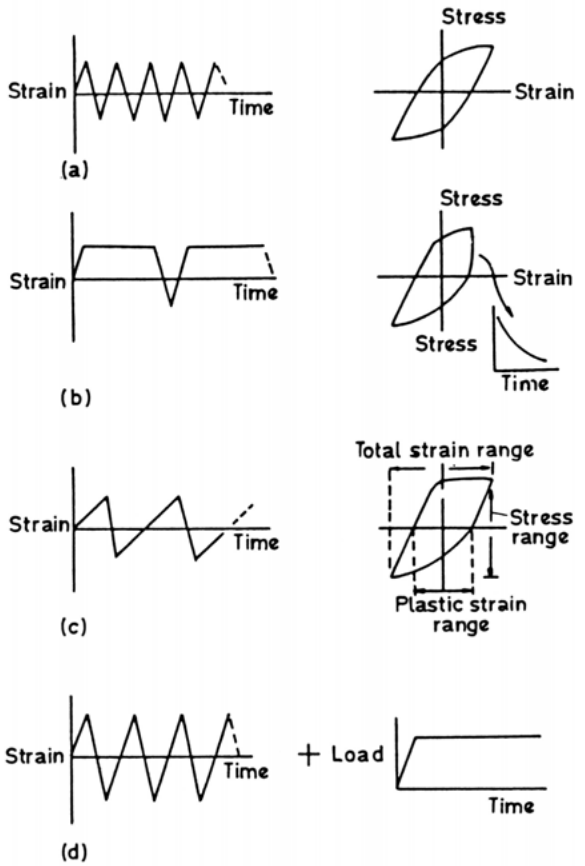

(a) Equal strain rate cycle (b) Tension hold period cycle
(c) Unequal ramp rate cycle (slow-fast)
(d) Sequential fatigue plus creep test

Fig. 1. Typical cyclic test waveforms

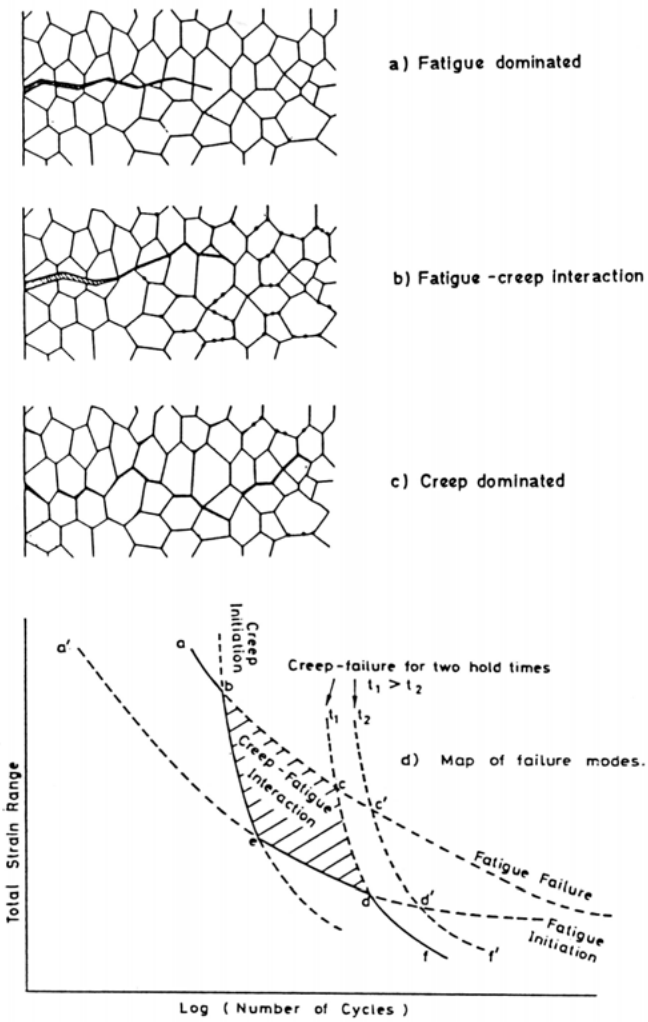

Fig. 2. Failure modes found during fatigue-creep testing and a map showing their regions of operation /7/

component of creep is usually introduced into the normal fatigue cycle (Fig. 1a) by means of a constant strain tensile (and/or compressive) dwell (Fig. 1b) or by reducing the tensile (or compressive) strain rate in the cycle (Fig. 1c); sequential fatigue-creep tests can also be performed, however /6/ (Fig. 1d). As the creep component of the cycle is increased by increasing the tensile dwell period, or by reducing the tensile strain rate, the failure mode of the material under test also changes. The failure modes observed can be categorised into three distinct regimes. These are:

1. Fatigue dominated;
2. Fatigue-creep interaction;
3. Creep dominated.

These three types of failure modes are shown schematically in Fig. 2 /7/.

Fatigue dominated failures arise due to the growth of surface fatigue cracks through the specimen, with no evidence of interaction with any creep damage, (Fig. 2a). During fatigue-creep interactions, creep cavitation damage is found within the material in addition to surface fatigue damage. Initially the fatigue crack growth rate is the same as that observed in a fatigue dominated fracture. However, eventually the fatigue crack interacts with the creep damage, resulting in accelerated crack growth, a reduction in endurance and a fatigue-creep interaction failure, Fig. 2b. Finally, under certain testing conditions, the creep component of the cycle dominates, and failures due to the accumulation of creep cavitation result. Under these conditions there is no interaction with any fatigue damage present, Fig. 2c.

One of the major aims of fatigue-creep testing is to predict both the endurance and the failure mode of specimens under any given set of testing conditions. This would enable the boundaries between the different failure modes to be established. It is important to know

these boundaries since any extrapolation of short term laboratory data is only valid provided it remains within one failure regime. It has already been qualitatively shown /7/ how such work could lead to the mapping of fatigue-creep behaviour in a manner similar to that already used for creep deformation and fracture /8, 9/, Fig. 2d.

The three failure modes described above have all been observed experimentally (see Section 2.3). In the next section the conditions under which these failure modes are observed for a range of engineering materials is discussed.

2.2. *Ferritic Steels*

High temperature cyclic/hold tests have been carried out on low alloy ferritic steels by a number of workers /10-16/. Ellison and co-workers /10, 11/ have performed simultaneous cyclic/hold tests on 1CrMoV steel at 565°C. These tests included either constant strain or constant load hold periods in tension and/or compression; the resulting data are shown in Fig. 3. [In Fig. 3 it should be noted that constant strain hold period tests are represented by t_1/t_2 where t_1 and t_2 are the hold times in minutes for tension and compression, respectively].

It was found that the addition of tensile dwell periods dramatically reduced the life of the material as compared with the continuous cycling case, the longer dwell periods leading to shorter lives. Metallographic studies /11/ showed that this decrease in life was associated with the initiation and growth of internal intergranular creep damage produced during the dwell periods; this damage gave rise to creep dominated failures.

Partial balancing of a tensile dwell with a shorter compressive dwell was seen to enhance the lifetime compared with the tension only dwell case, whilst equal tension and compression dwells gave lifetimes approaching those of pure fatigue tests. These observations are explained by the fact that the inclusion of the compressive dwell reduced the amount of internal intergranular creep damage compared with that found in tension only dwell tests. For equal tension and compression dwells, internal creep damage was reduced to negligible proportions and failure was fatigue dominated. In these latter tests, the creep damage formed during the tensile dwell was fully reversed during the compressive dwell, resulting in increased endurance.

It is important to note that metallographic examination of interrupted and failed specimens from these tests indicated that the fatigue and creep damage processes were, in the main, acting independently of each other /11/, (Fig. 4). This will be seen to be

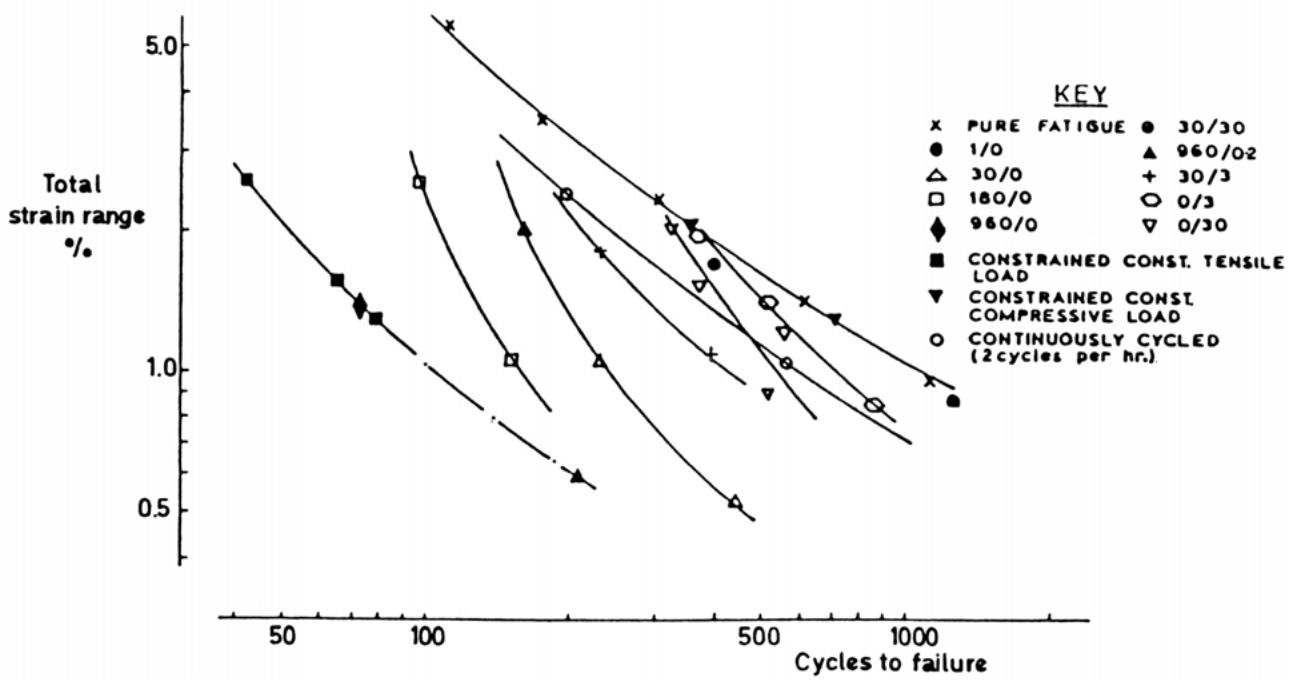

Fig. 3. Plot of total strain range vs. cycles to failure for 1CrMoV steel at 565°C /10/

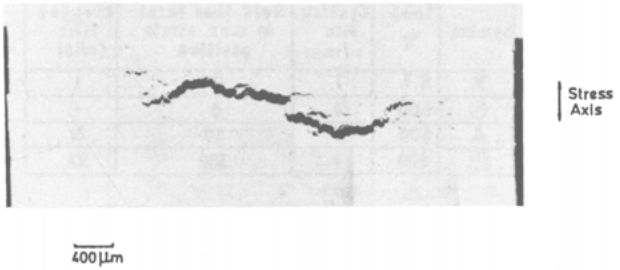

Fig. 4. (a) Void profile at failure in 30 min. tensile dwell test (1CrMoV steel, 565°C /11/)

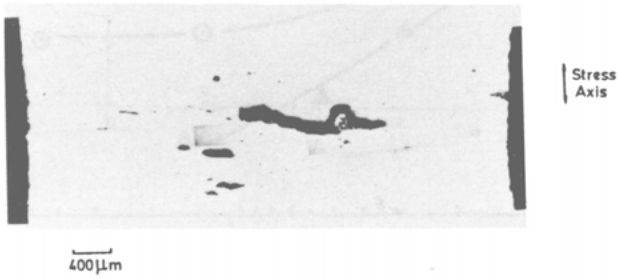

Fig. 4. (b) Void profile at failure in 30 min. compressive dwell test (1CrMoV steel, 565°C /11/)

an important consideration when different life prediction techniques are assessed using the 1CrMoV steel fatigue-creep data shown in Fig. 3.

Batte *et al.* /12/ have performed cyclic/hold tests on a ½CrMoV steel at 500, 525 and 550°C; tensile dwell periods of up to 16 hours duration were used in these reverse-bend tests. As with the 1CrMoV steel data /10/, tensile dwell hold periods included at the maximum tensile strain resulted in the largest reduction in endurance. In addition, creep dominated failures were apparent for the long term tests (16 hours dwell, total strain range $< 1.0\%$), once more in agreement with the 1CrMoV steel data. At total strain ranges of greater than 1.0%, the failure mechanism changed to fatigue-creep interaction.

Similar behaviour to that exhibited by 1CrMoV steel has recently been observed in 1Cr-½Mo steel by Miller and Gladwin /15/. Testing at 535°C and under 16-hour tensile dwell conditions, creep dominated failure was observed. Material tested in the parent and simulated heat affected zone heat treated conditions showed that the latter had the lowest endurance, in line with the lower ductility exhibited by this microstructural condition.

In contrast to the above data of 1CrMoV, ½CrMoV, and 1Cr-½Mo steels, Wood *et al.* /17/ found that the endurance of 9% Cr steel tested at 525°C was not strongly affected by the introduction of a tensile dwell period into the cycle. The 9% Cr steel was characterised by a high creep ductility, and no evidence of intergranular cracking in the tensile dwell period tests was found. This observation thus explains why only a small reduction in endurance was found in the dwell tests on the 9% Cr steel.

In contrast to 1CrMoV, and 1Cr-½Mo steels, observations on 2¼Cr-1Mo steel /14/ revealed that tensile dwells had little effect on endurance. However, it was shown that a compressive dwell period could be very detrimental with respect to endurance. Recently Challenger *et al.* /18/ have explained these results in terms of oxidation effects. They suggest that during compressive dwells, oxide growth occurs. This is followed by a relatively large tensile strain, equal to the total strain range of the test, as the specimen is cycled. The cyclic excursion is thought to crack the oxide, thereby causing the large life reduction observed, this model also explaining the observation of circumferential oxide cracking. In this context it is worth noting that Brinkman *et al.* /14/ performed their tests under diametral strain control. Clearly, in the presence of significant oxidation, such testing is open to error. Further, the dwell periods examined in this study were to a maximum of 6 minutes and, clearly, longer term dwell data are required in order to clarify the true behaviour of the 2¼Cr-1Mo steel. Indeed, other data on a 2¼Cr-1Mo steel /19/ have shown that, as expected, tensile dwells can be damaging (Fig. 5). In this latter work, long hold periods of 30 and 300 minutes were employed compared with the short dwells used by Brinkman *et al.* /14/. On this evidence, it would appear prudent to re-test specimens of the type used by Brinkman *et al.* /14/, this time using axial strain control with longer hold times, to see if the unexpected results reported for 2¼Cr-1Mo steel are indeed representive.

From this brief review of ferritic steel fatigue-creep behaviour, it is apparent that one controlling material parameter that strongly influences endurance is the creep ductility. An attempt to demonstrate this is illustrated in Fig. 6, which shows endurance data for several ferritic steels in relation to the range of creep ductility exhibited by them. Also, where information is available, the observed failure mode associated with each data point is given in Fig. 6. From this figure, it is evident that the lower the ductility, the lower is the fatigue-creep endurance. In addition, it is clear

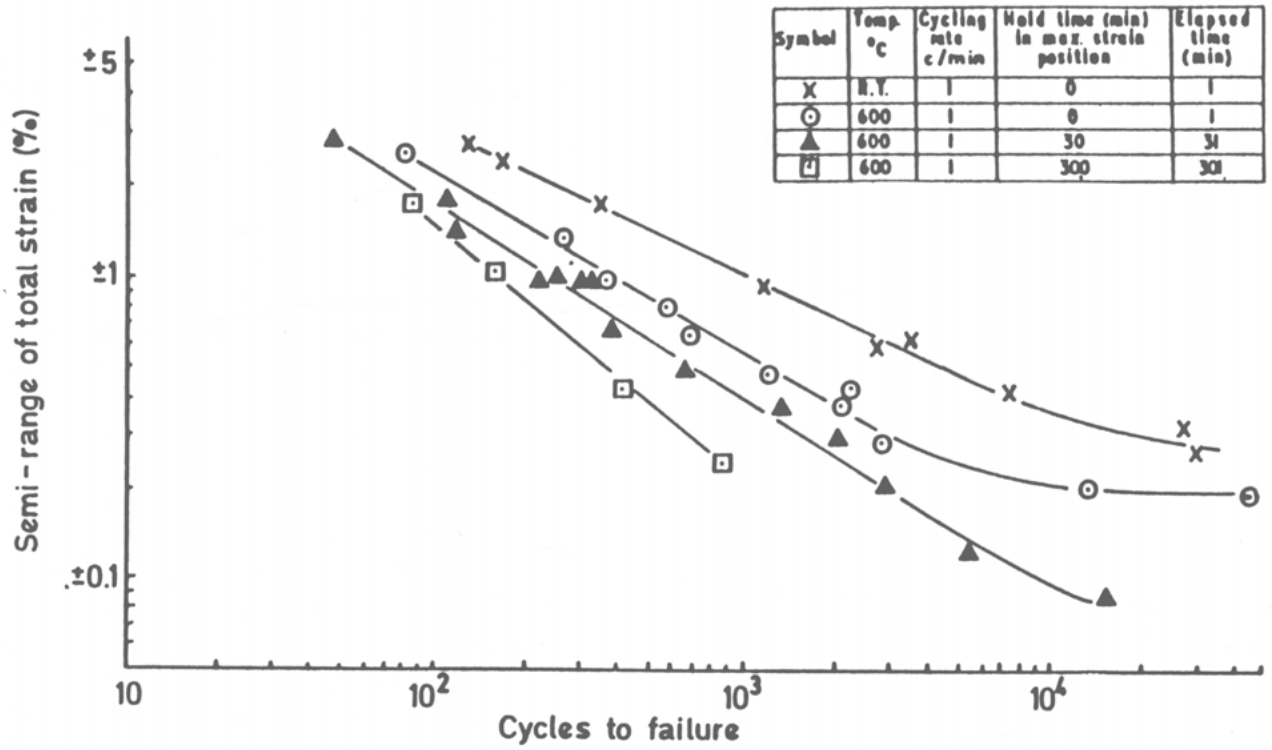

Fig. 5. Reversed bending tests on 2.25% Cr — 1% Mo steel, showing effect of temperature and hold time at maximum strain /9/

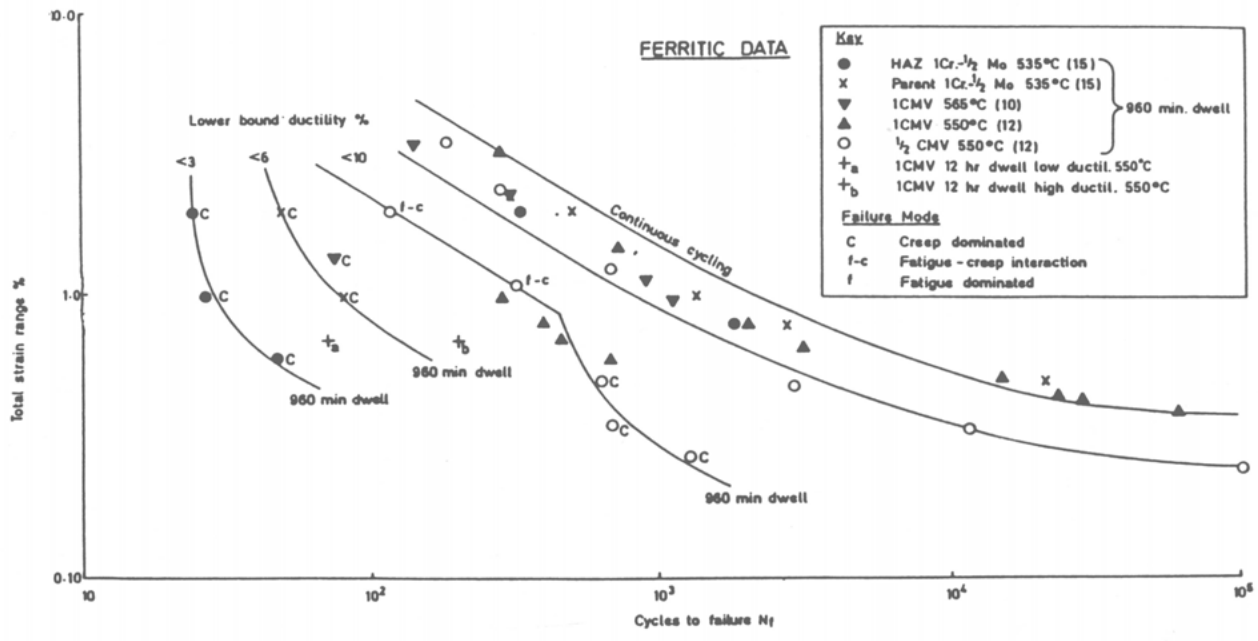

Fig. 6. Effect of ductility on endurance in ferritic steels

that long dwell periods, small strain ranges and low ductility favour creep dominated failure, whereas intermediate strain ranges, short dwell periods and high creep ductility favour fatigue-creep interaction failures.

2.3. *Austenitic Stainless Steels*

A large amount of data is available in the literature on the fatigue-creep behaviour of austenitic stainless steels, in particular types 316 and 304. This is due

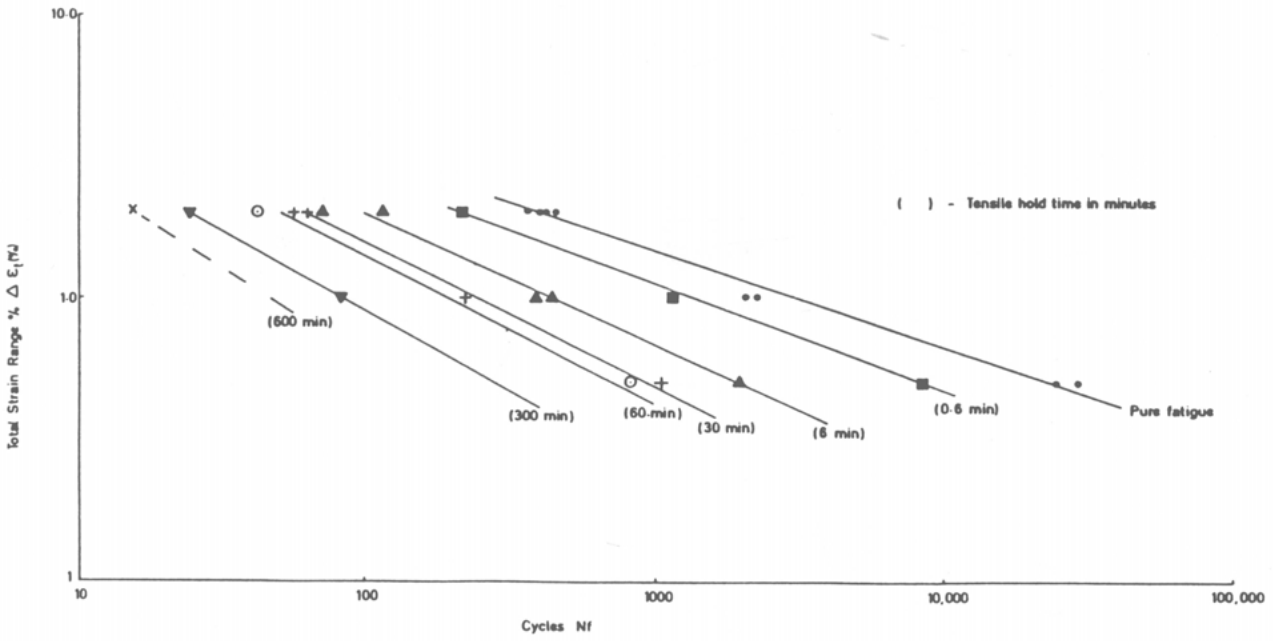

Fig. 7. Fatigue-creep data on 316 steel-tensile only dwells /21/

to their extensive use in nuclear power plant. Initial studies on type 316 stainless steel /20-26/ revealed that in the temperature range 550-625°C, tensile dwell periods were most damaging; the longer the hold period, the more damaging the cycle, (Fig. 7). However, the failure mode observed was often identified as fatigue-creep interaction (Figs. 2b and 8), in which the fatigue crack interacted with creep damage, causing an accelerated crack growth rate and a reduction in endurance. These observations are unlike those reported previously in 1CrMoV /11/ and 1Cr-½Mo /15/ ferritic steels which exhibited creep dominated failures. Unfortunately, most of the earlier work on austenitic steels was conducted using short dwell times at intermediate strain ranges (i.e. total strain ranges $> \pm 0.7\%$), and it is only recently that data on austenitic stainless steels have been obtained for long dwell periods ($\sim$ 1000 mins) and small total strain ranges ($< 0.6\%$). Such data have revealed that creep dominated failures also occur in austenitic stainless steel /27-29/. Goodall *et al.* /27/ have reported creep dominated failures in type 316 stainless steel for total strain ranges of 0.6%, when tested at 600°C with tensile dwells of 100 and 1000 minutes. Wood *et al.* /28/ have also reported creep dominated failures following tests at 625°C which included 2880 minute dwell periods. Another important parameter dictating failure mode and hence endurance is the cast to cast variation in the ductility of 316 stainless steel /30/. Recently, Wareing /29/ has investigated the fatigue-creep properties of four casts of 316 stainless steel, using dwell periods of up to 1440 minutes and total strain ranges in excess of 0.6%. It was found that the extent of life reduction varied from cast to cast, and that a correlation existed between stress-rupture ductility and the maximum fatigue-creep life reduction factor. Therefore, it is important to note that any one set of data obtained from a cast of 316 stainless steel will not necessarily reflect the typical behaviour of that material. Indeed, some workers /24, 29/ have observed a saturation in the detrimental effect of tensile hold periods, a recovery of the endurance being observed as the hold period was extended further. This effect has been related to microstructural ageing processes taking place during the test, which subsequently influenced material properties such as cavity nucleation rate and creep ductility. Compressive hold periods have been shown to have a similar effect on stainless steels /13/ as that observed in 1CrMoV steel /11/.

A number of studies /32-35/ have investigated the fatigue-creep behaviour of stainless steels, such as types 304, 316 and 20%Cr/25%Ni/Nb, by using slow-fast cycles (Fig. 1c). In these studies it was found that reducing the tensile strain rate in the cycle resulted

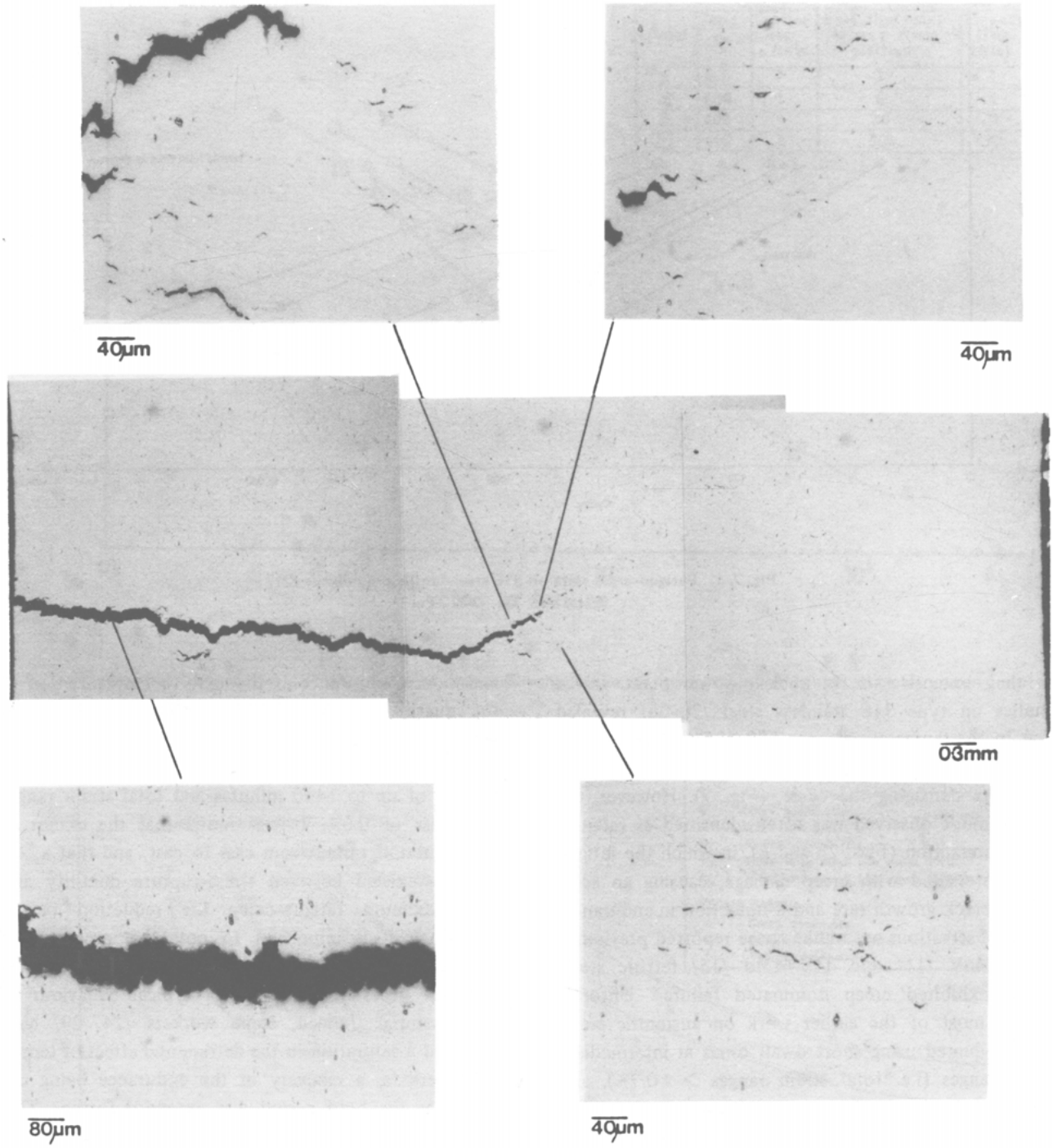

Fig. 8. Fatigue–creep interaction failure in 30 min. tensile dwell test on 20/25/Nb stainless steel tested at 650°C /35/

in a reduction in endurance. Coincident with this was a change in failure mechanism from fatigue dominated, to fatigue-creep interaction to creep dominated failures at very low strain rates. Data on a 20/25/Nb stainless steel produced at 650°C are shown in Fig. 9, from Gladwin and Miller /35/. The failure mode of each test is indicated as previously. It was found that at tension/compression strain rates of $10^{-6}/10^{-3}s^{-1}$, and strain ranges less than 2%, failure was by fatigue-creep interaction (Fig. 10). In contrast, as strain rates

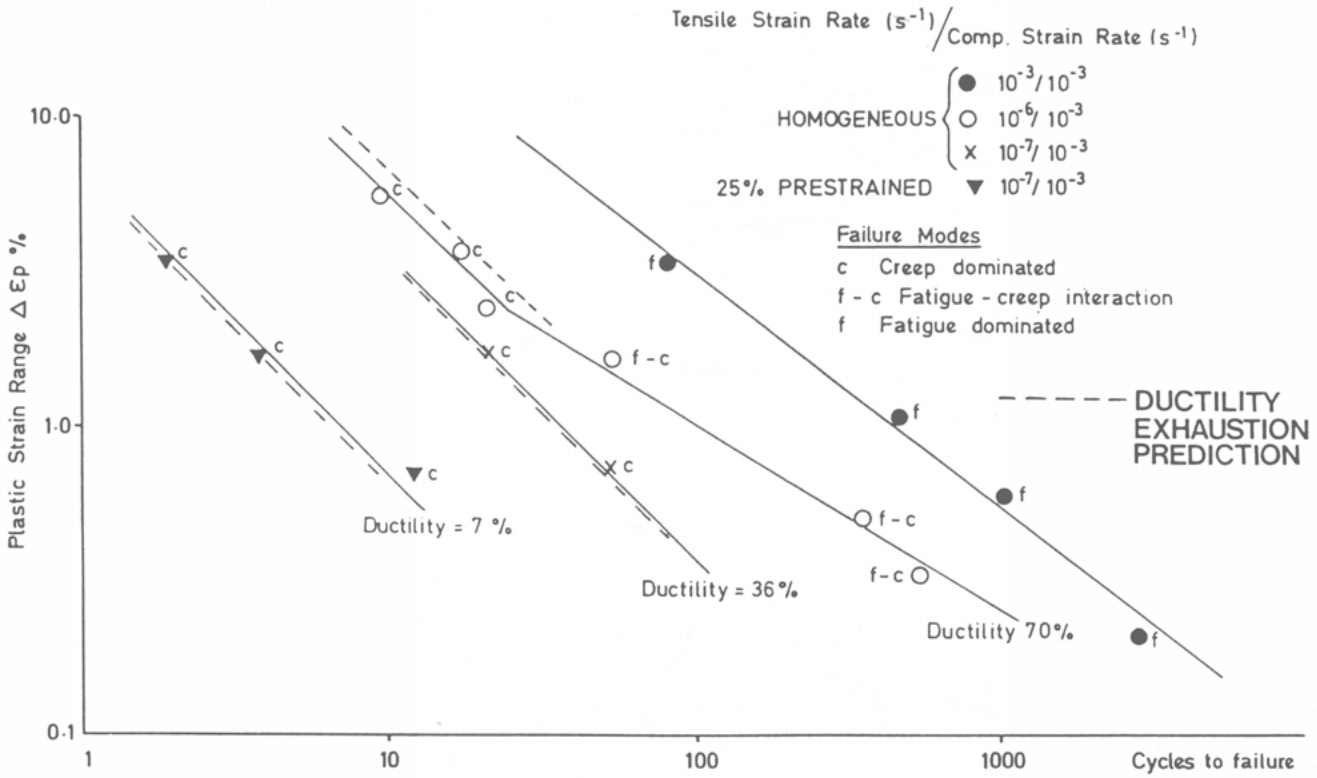

Fig. 9. Slow-fast endurance data for 20/25/Nb steel at 650°C /35/

of $10^{-7}/10^{-3}s^{-1}$ (and $10^{-6}/10^{-3}s^{-1}$ at strain ranges $> 2\%$) failure was by a creep dominated mechanism (Fig. 11).

Additional data are included in Fig. 9 from pre-strained material which exhibited a lower creep ductility. From Fig. 9, the strong influence of ductility on the endurance of the 20/25/Nb steel at 650°C can be seen. It should be noted that in the slow-fast cycle, ductility data are only required at the slow tensile strain rate, and it is therefore most convenient to show the effect of this parameter on endurance by using these cycles. The ductilities for the other test and material conditions are also included in Fig. 9.

2.4. Nickel Base Alloys

There is a considerable amount of evidence to indicate that in many nickel base alloys, the compressive strain dwell is more detrimental than the tensile dwell period. This behaviour was shown by Ostergren /36/ for Cast IN738; by Hyzak and Bernstein /37/ for Rene 95; by Antunes and Hancock /38/ for MAR M002; and by Lord and Coffin /39/ for Cast Rene 80. Kortovich and Sheinker /40/ tested Rene 80 at 1000°C and observed that, whereas transgranular cracking resulted solely from cyclic straining, both the tensile dwell and compressive dwell tests showed intergranular cracking, the latter having the shorter life.

Wells and Sullivan /41, 42/ appear to have been the first workers to note the unexpectedly damaging effect of compressive dwells. They suggested that the tensile stress in the cycle promoted the growth of round cavities, whilst under compressive stress the cavities grew into elongated flat cracks. Since the work required to fracture a grain boundary is greater when the boundary contains round cavities, both because the stress concentration at each cavity is smaller than for flat cracks and because they may also comprise a smaller fraction of the grain boundary, it was argued that compressive dwells should be most damaging. This proposal clearly requires further study, though it is pertinent to point out that no really satisfactory mechanistic explanation for the damaging compressive hold tests has yet been put forward.

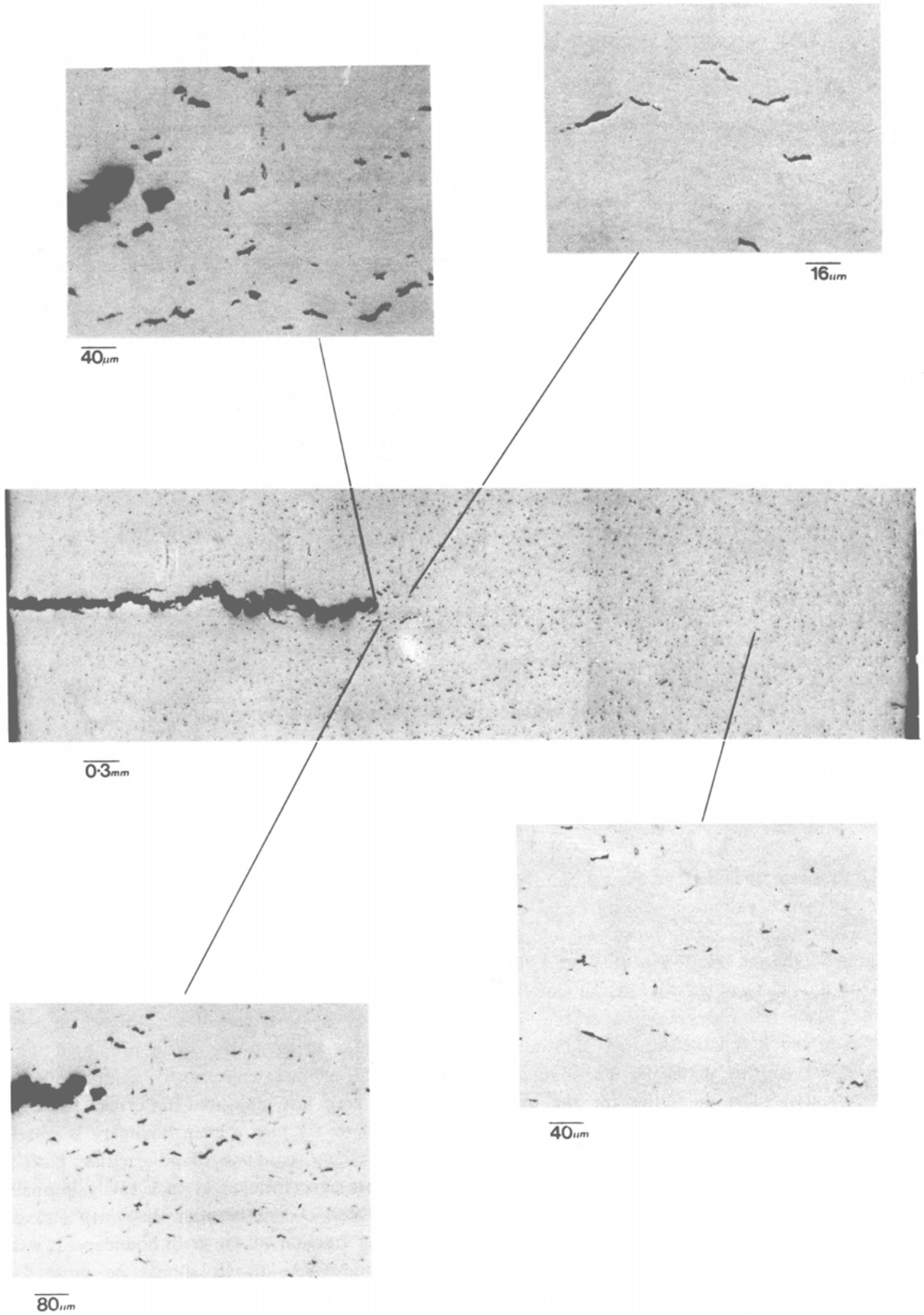

Fig. 10. Fatigue–creep interaction failure in 20/25/Nb steel /35/

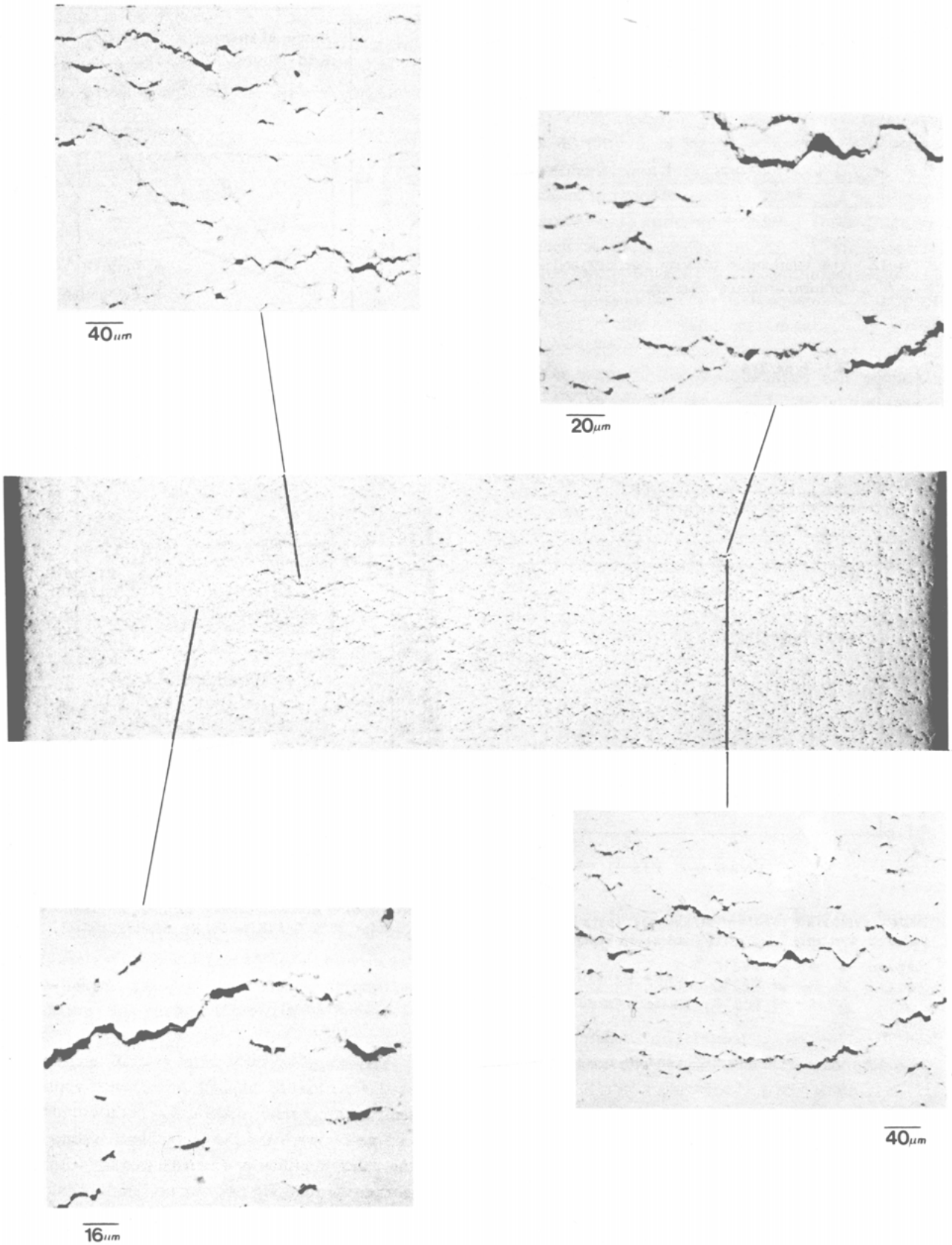

Fig. 11. Creep dominated failure in 20/25/Nb steel /35/

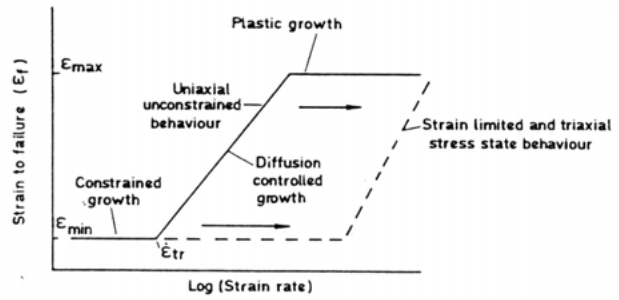

Fig. 12. The relationship between ductility and strain rate for many structural materials

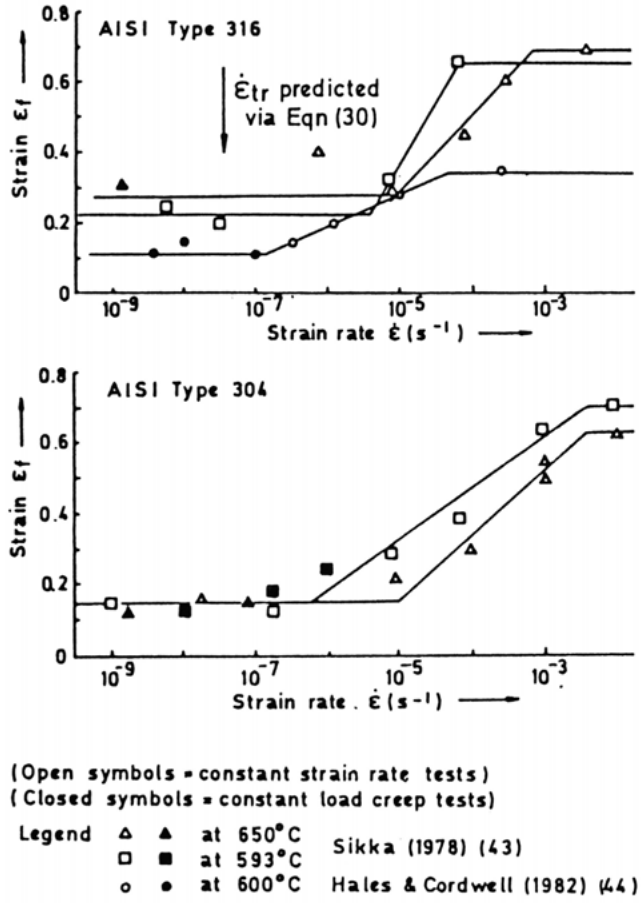

Fig. 13. Variation of ductility (ϵ_f%) with strain rate or stress for a number of engineering alloys /107/

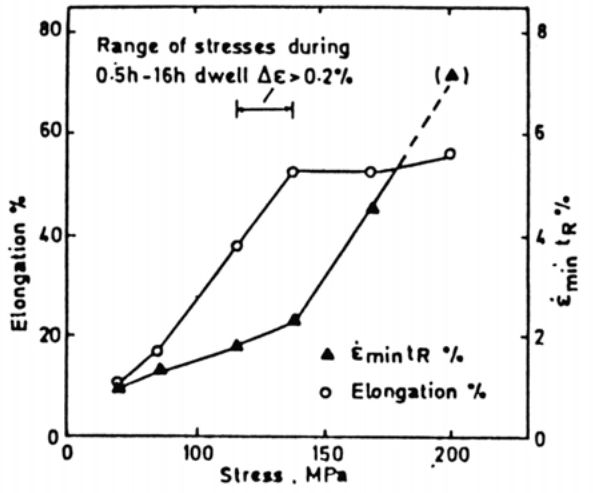

Stress dependence of creep ductility at 550°C for ½ Cr MoV (46)
Note difference between Elongation and $\dot{\varepsilon}_{min} t_R$ values

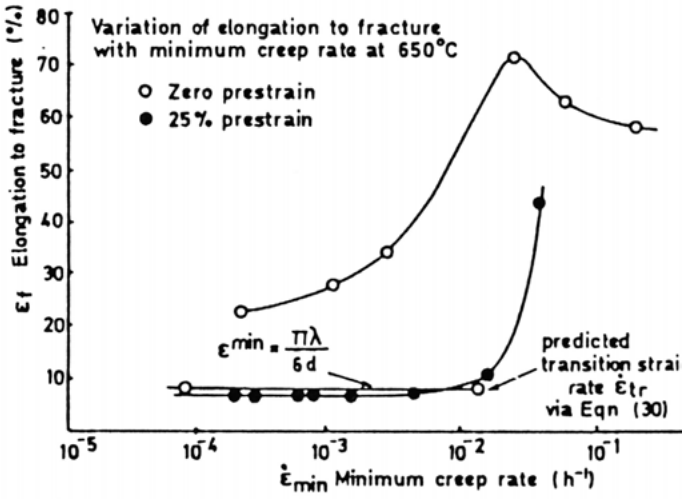

Plot of creep ductility against minimum creep rate for 20% Cr/25% Ni/Nb Stainless steel

Fig. 13 (cont)

2.5. *Ductility*

In the last few sections it has been shown that fatigue-creep endurance is strongly influenced by material ductility. It is therefore prudent to briefly discuss some aspects of this parameter.

The creep ductility of a material is known to vary as a function of applied rate (hence applied stress), temperature, microstructural condition, stress state and cast. In general, under uniaxial testing conditions the creep ductility is observed to vary with strain rate as indicated in Fig. 12. As the strain rate is reduced, the ductility reduces from a high plateau level, through some transition region to a low minimum ductility level at low strain rates. This behaviour is shown in Fig. 13 for a number of different engineering alloys

/43-47/, and can be explained in terms of our current understanding of cavity growth mechanisms. The variation of cavity growth rate with stress is shown in Fig. 14; as the stress is reduced the growth mechanism

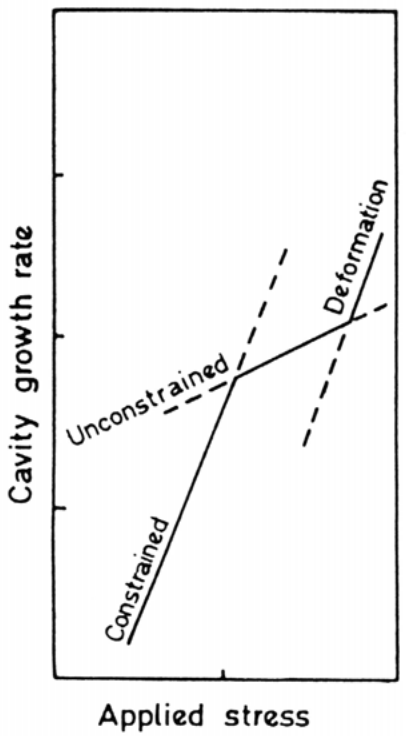

Fig. 14. Cavity growth rate as a function of applied stress; the continuous line follows the rate controlling path

changes from deformation /48/ to unconstrained /49, 50/ to constrained /51/ cavity growth. This latter process is very efficient in converting plastic strain into cavitation, resulting in ductilities of a few percent /51/ at low strain rates/stresses. Increasing the applied stress ultimately changes the rate controlling mechanism to unconstrained growth and then to deformation growth. During this change, the strain to fracture increases since the latter two mechanisms require greater specimen strain before cavity coalescence occurs. In the case of deformation growth, fracture strains in excess of unity can occur. When this mechanism operates, fracture invariably occurs by an alternative mechanism (i.e. transgranular fracture).

In a tensile dwell period, a range of strain rates are encountered. If they are greater than $\dot{\epsilon}_{tr}$, shown in Fig. 12, then endurance will not be severely reduced. Such conditions may be met, for example, during short dwell periods. However, as the dwell period increases, the strain rates encountered are likely to be less than $\dot{\epsilon}_{tr}$. The low ductility constrained cavity growth mechanism can then operate, giving rise to large reductions in endurance. It will be seen in section 3.5 that a knowledge of this transition rate from low to high ductility is of use when attempting to model damage accumulation during dwell periods.

However, in order to apply ductility data to fatigue-creep analyses, a further complication arises. Ductility data, such as those shown in Fig. 13, are generally determined from uniaxial loading conditions (i.e. macroscopically unconstrained). Consequently, for high ductilities (> 30%), significant necking can occur during the tertiary region of the creep curve; in strain controlled tests, no such instabilities can occur. It has also been shown that creep rates during dwell periods are different from those obtained during creep tests at comparable stresses. For example, for ½CrMoV steel tested at 550°C /46/, (Fig. 15), it was observed

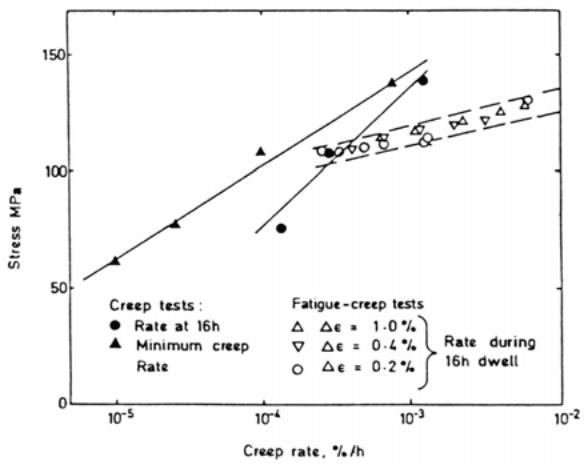

Fig. 15. Creep rates during steady-load creep and fatigue-creep hold periods at 550°C /46/

that the stress exponent changed from 2-4 in creep tests to 15-20 in the dwell period tests. In addition to this difference in deformation behaviour, it has also been observed /46, 52/ that creep cavitation damage is present at higher stresses and strain rates in fatigue-creep testing than in creep tests. This observation suggests that the ductility behaviour shown in Fig. 13 for uniaxial load controlled conditions is changed under macroscopically constrained (i.e. strain limited) conditions. A possible change is suggested in Fig. 12, in that the low ductility region (constrained cavity growth) operates at higher stresses; this would be in agreement with the above observations. The difference

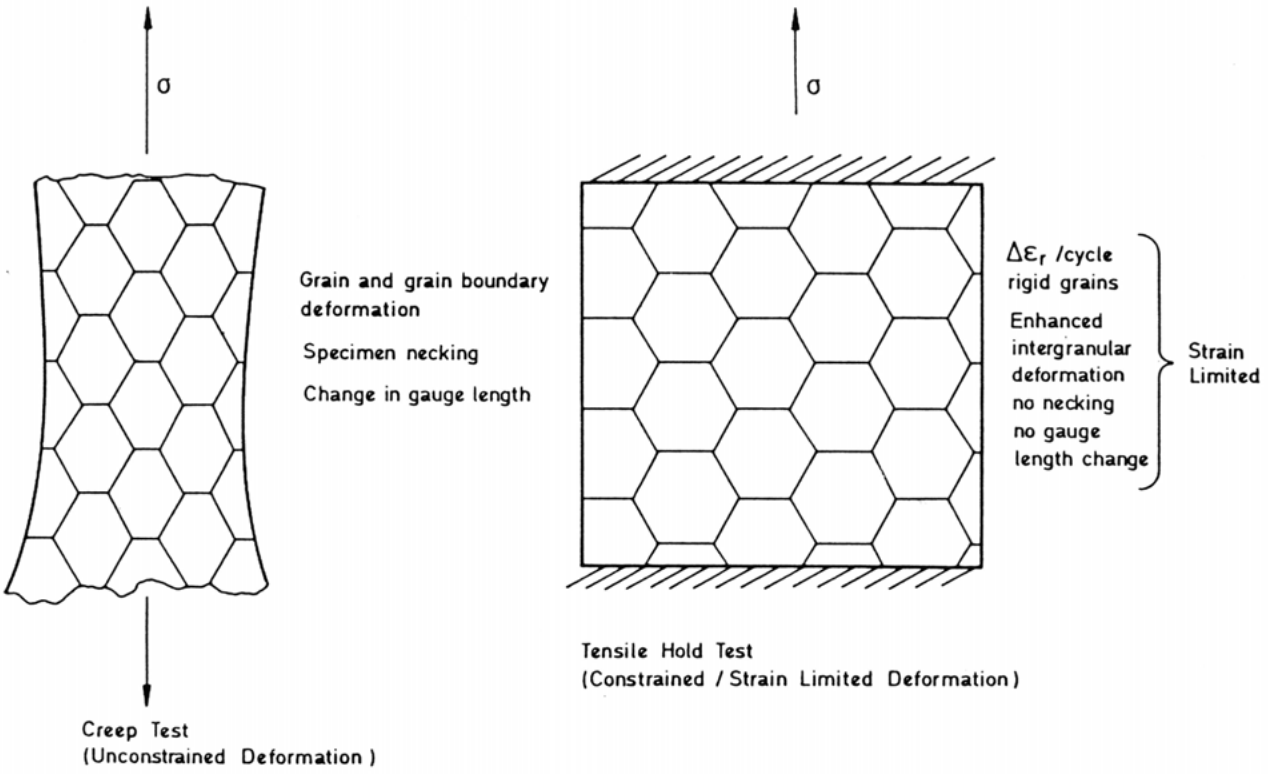

Fig. 16a. Schematic representation of unconstrained and strain limited deformation

between unconstrained (i.e. creep tests) and strain limited (constant strain stress relaxation) deformation is depicted schematically in Fig. 16a. In the former case the grains are free to deform, and therefore the relationship between intergranular and transgranular deformation will be dependent on microstructure, stress and temperature. In the strain limiting case, the plastic strain relaxes in a material in which the grains are not free to deform. It is suggested that under these conditions the strain occurs predominantly at the grain boundaries, thereby enhancing intergranular damage in the strain limiting case; this is in agreement with experimental observations.

Experimental evidence demonstrating the effect of constrained (strain limiting) conditions on ductility is limited. However, the effect of triaxiality on ductility is similar to that caused by strain limited testing conditions. Fortunately, data are available on the effects of stress state on ductility, and these are shown in Figure 16b for Nimonic 80A /53/. Fig. 16b clearly shows the expected reduction of ductility under triaxial stress conditions. Thus it is clear that a number of factors can influence ductility data, and their applicability to fatigue-creep analyses must be used with caution.

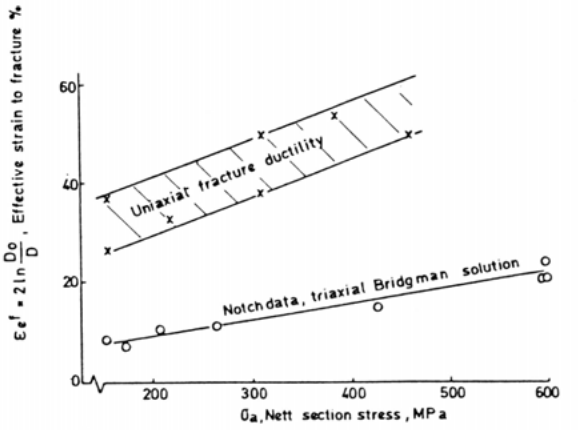

Fig. 16b. Fracture ductilities of notched specimens are lower than uniaxial ones at all stress levels /53/

2.6. *Environment*

The work of Coffin /54/ and White /55/ indicated the importance of environment, especially the presence of oxygen, in the life of specimens tested at elevated temperature. Indeed, Coffin /54/, and Solomon and Coffin /56/ showed that oxidation effects could be more important than time dependent creep mechanisms for an iron based superalloy A286 at 593°C.

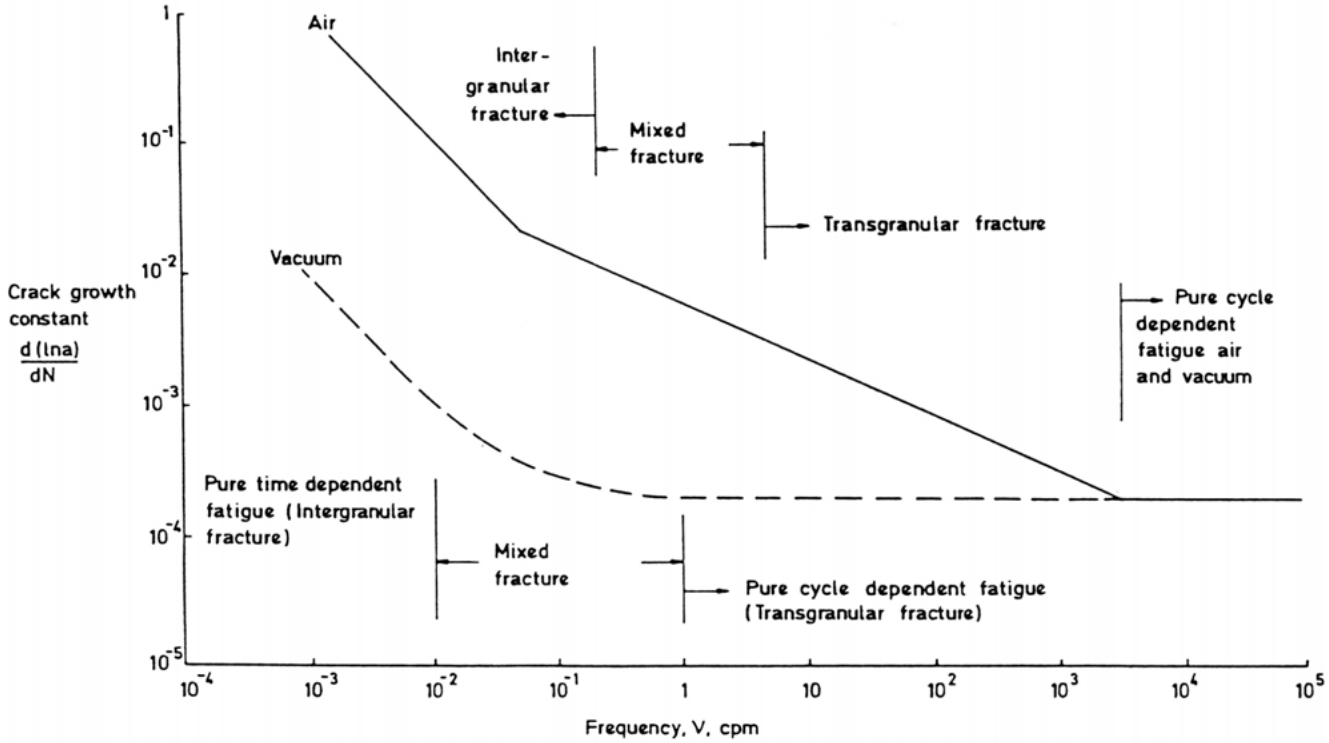

Fig. 17. Comparison of air and vacuum crack growth behaviour for Fe-Ni alloy A286 at 593°C /56/

They found an order of magnitude increase in endurance for tests conducted in vacuum, compared with those in air. The alloy showed a distinct frequency effect and the cracking mode was intergranular in air, whilst in vacuum there was negligible frequency effect and cracks were transgranular. The implication was that oxidation of the surface provided initiation sites for cracks and then increased crack growth rates. A schematic plot of the crack growth rates versus frequency is shown in Fig. 17. In air at very high frequencies, crack propagation is due to frequency independent fatigue with transgranular fracture. However, as the frequency is decreased, the environmental effects interact with the fatigue process, thereby increasing the crack growth rate. At still lower frequencies, the influence of pure time dependent processes becomes dominant, resulting in intergranular fracture. In vacuum, the environmental influence on the fatigue processes is removed so that transgranular cracking occurs over a larger frequency range; however, the pure time dependent process is still dominant at the very low frequencies. Coffin has analysed additional data for Udimet 500 and AISI 304 stainless steel and found similar effects; information on other alloys can also be found /54/.

Similar trends have been observed in type 316 stainless steel by Wood *et al.* /57/ and by Levaillant, Rezqui, Pineau /58/. The longer lives obtained in the inert atmosphere were attributed to increased resistance to crack initiation and a reduced rate of crack propagation. Further elevated temperature tests on 347 stainless steel and Hastalloy X in air and hydrogen gas showed longer lives in hydrogen, particularly at the highest test temperature /59/. There has also been considerable interest in the nuclear power industry, on the effect of sodium on stainless steels, particularly type 316, because of their use in cooling circuits. It has been found that air generally has a more detrimental effect on endurance than does sodium /60/.

However, environmental effects are not always as straightforward. Continuous cycle and tensile hold tests on 304 steel, performed in air and vacuum at 1200F by Harrod and Manjoine /61/, showed that there was no environmental effect. Earlier work by Gell and Leverant /62/ on the nickel base alloy MAR M200 showed both beneficial and detrimental effects of vacuum on life. For example, in room temperature tests the life in air was less than in vacuum, but for tests at 910°C the reverse was true. This unexpected result was found to be due to oxidation blocking the initiation of cracks, thereby making them less effective. For the nickel base alloy IN738LC in cast and wrought

forms, Scarlin /63/ compared cracking behaviour in air and vacuum. The cast alloy had a slightly decreased rate of crack propagation in air relative to vacuum, because of crack bifurcation following selective oxidation of dendritic boundaries; in contrast, the wrought alloy suffered accelerated crack growth in air because of the preferential oxidation at the grain boundaries, as for the Udimet 500 mentioned earlier.

Referring back to the concept of oxide blocking, it is useful to consider the study of threshold stress intensities for crack growth by Haigh *et al.* /64/. Using tests on a 1CrMoV steel at 550°C over a range of frequencies, Haigh *et al.* /64/ found that in air the threshhold increased with decreasing frequency, reflecting the presence of oxide blocking the crack and therefore reducing the effective stress intensity. However, above the threshold, the oxidation at the grain boundaries was seen to increase the crack propagation rate.

It is thus not easy to generalise on the influence of the environment on different alloys, except to say that whereas grain boundaries are oxidation sites for crack initiation, in an inert environment cracking is usually transgranular if time dependent creep mechanisms are absent. As Tomkins /65/ has pointed out, the role of environment is complex because it depends on both material and mechanics. The material effect is related to the environment/material interactions, surface chemistry, diffusion and internal reactions. Mechanics considerations are associated with reversibility of the shear decohesion and wedging in the crack, and the ability to renew the crack tip environment. As already seen, the presence of an oxidising environment can cause either acceleration or deceleration of crack growth; acceleration due to metal at the crack tip being replaced by oxide which is cracked in the next cycle, so causing a fast propagation rate, deceleration due to oxide blocking or wedging.

Attempting, finally, to compare the relative effects of the two time-dependent effects of environment and creep it appears that, whereas oxidation can cause increases in crack propagation rates by up to an order of magnitude, creep processes can lead to two or three orders of magnitude increase in crack growth rate. The similarity, of course, is that both the oxidation and creep damage processes lead to intergranular cracking, and therefore usually to a decrease in life compared with fatigue and its transgranular mode of cracking. For simplicity, the remainder of this review will be restricted to looking at time dependent creep damage rather than environmental effects. A survey of the currently most popular life prediction techniques to cater for fatigue-creep situations follows.

3. LIFE PREDICTION TECHNIQUES

The question facing any designer of plant which operates in the combined fatigue-creep regime is how to *add* the damage processes of fatigue and creep to produce a life equation.

The study of life prediction for components subject to simultaneous cyclic and creep deformation has led to the development of several possible techniques for design purposes. The most widely used approach is based on the linear superposition of fatigue and creep damage; indeed, the mainstay of present design procedures that account for creep and fatigue damage is the linear life fraction rule which forms the basis of the ASME Boiler and Pressure Vessel Code, Section III, Code Case N-47 /5/. However, continuous damage approaches which aim to describe the interaction of the progressive deterioration processes on a continuum basis are also being developed /66-69/.

The continuum damage methods are stress based, and as such are particularly sensitive to errors, damage being proportional to stress raised to a high power. Although, in theory, these techniques should be particularly useful in modelling any interaction between creep and fatigue, in practice poor agreement with observed data has resulted /70/. Such stress based approaches will not be pursued further in this review. Instead, only the most popular of the remaining methods will be described in this section. These will also be assessed against fatigue-creep test data obtained from a range of sources.

3.1. Linear Life Fraction

This approach combines the damage summations of Miner /71/ and Robinson /72/ as proposed by Taira /73/. It describes a linear summation of the separated time-independent and time-dependent damage and is given by:

$$\Sigma \frac{N}{N_p} + \Sigma \frac{\tau}{T_d} = 1 \qquad (1)$$

where N/N_p is the cyclic part of the life fraction in which N is the number of cycles at a given cyclic strain range and N_p the pure fatigue life at the same strain range. The time dependent fraction is τ/T_d, in which

τ is the time at a given stress and T_d is the time to rupture under static creep loading at the same stress. The simple summation is given to unity.

A brief analysis of results from several sources indicates the potentially inaccurate nature of this method in assessing damage. For example, Priest *et al.* /70/ showed that 1CrMoV steel tested at 565°C exhibited a wide spread of data on both sides of the damage summation line, (Fig. 18a). Wood *et al.* /28/, who carried out strain controlled cyclic/hold tests at 625°C on a 316 stainless steel, also showed that a substantial number of their results lay above the damage summation line. Thus, although conservative predictions would have been obtained, confidence in the linear damage approach was not supported. However, a bi-linear damage line appeared to provide an approximate lower bound for these particular data, (Fig. 18b; see Section 4). Similar scatter for Alloy 800 and Type 304 stainless steel has been correlated by Jaske *et al.* /74/, with effective values for the damage summation varying from 0.2 to 10, instead of unity. Maiya /75/ has also obtained poor predictions for a type 304 stainless steel.

Some workers /12, 17, 76/ have obtained agreement to within a factor of two between predicted and observed lifetimes for different low alloy ferritic steels. However, these assessments have included modifications which take account of the initial rapid strain accumulation during the hold periods /12/. Further, the "apparently" correlated data of Wood *et al.* /17/, (Fig. 18c), whilst indicating that conservative predictions would have been obtained using the life fraction approach, once more gives little confidence in the overall accuracy of this method. Indeed, the uncertainty of the method is itself reflected in the need for differing values of the damage summation, as advocated in ASME Code Case N-47 /5/ (see Section 4.2).

The major advantage of the linear life fraction approach, however, is that it is simple to apply. Despite this, the approach is phenomenological, having no real mechanistic basis, and its applicability is therefore material dependent. In addition, with the linear life method tensile and compressive hold periods are equally damaging, and no account is taken of the "healing" effect of compressive dwells on prior tensile dwells /10/.

A further potential advantage of the life fraction approach is that it requires only simple fatigue and constant stress creep rupture data for its application. However, sequential fatigue-creep test data have shown that creep behaviour can be considerably affected

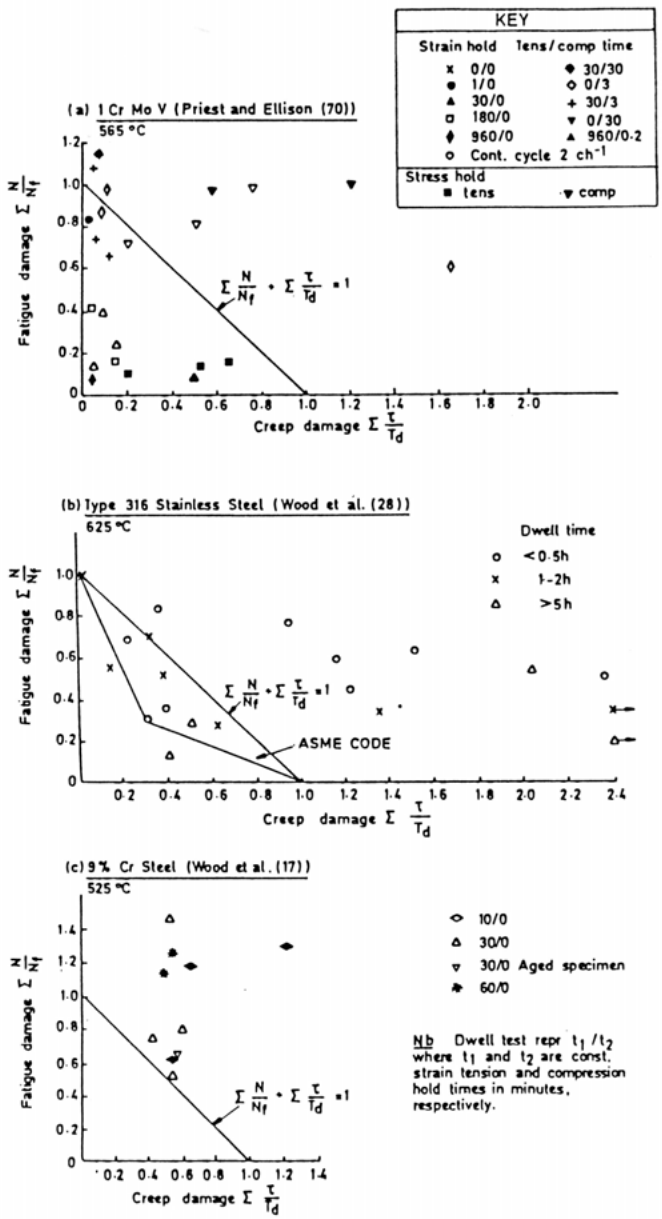

Fig. 18. Linear life fraction

by prior cyclic plasticity, and the use of virgin creep data in equation (1) may be inappropriate /70/.

3.2. Frequency Separation

This method is a direct extension of the familiar Manson-Coffin relationship

$$\Delta\epsilon_p N_f^{\alpha} = \text{const.} \qquad (2)$$

where $\Delta\epsilon_p$ is the inelastic strain range, N_f the number of cycles to failure and α a constant.

Coffin /3, 54, 77/ has developed several methods

to take account of environmental and other time dependent effects in fatigue at high temperature, by the introduction of a frequency term into the Manson-Coffin law. In particular, to cater for severely unbalanced loop shapes, he devised the frequency separation approach /77/. With this approach, complex hysteresis loops containing hold periods were assumed to be approximated by continuous loops with constant, though different, tension and compression going strain rates (ν_t and ν_c); it should be noted, however, that some workers /78/ have raised doubts about the equivalence of unequal ramp rate tests and dwell tests. This led Coffin to a lifetime equation of the form:

$$N_f = [\frac{A'}{\Delta\sigma_{sf}}]^{1/\beta'} [\frac{\nu_t}{2}]^{K_1'/\beta'} \quad (3)$$

where A', β', and K_1' are coefficients from the Basquin relation

$$\Delta\sigma = A' N_f^{-\beta'} \nu^{K_1'}$$

ν is the cyclic frequency and $\Delta\sigma_{sf}$ is the stress range for loops with unequal ramp rates, given by

$$\Delta\sigma_{sf} = \frac{A}{2} \Delta\epsilon_p^{n'} [(\frac{\nu_t}{2})^{K_1} + (\frac{\nu_c}{2})^{K_1}] \quad (4)$$

Here n', A and K_1 are constants in the second Basquin relation /3/

$$\Delta\sigma = A \Delta\epsilon_p^{n'} \nu^{K_1} \quad (5)$$

and ν_t and ν_c are the tensile and compressive frequencies, respectively. The frequency separation technique used coefficients obtained from balanced loops only. Coffin /77/ pointed out that this may not always be possible and derived a similar equation which used some hold time data also:

$$N_f = [\frac{F}{\Delta\epsilon_p}]^{1/\beta} [\frac{\nu_t}{2}]^{1-K} [\frac{\nu_c}{\nu_t}]^{d} \quad (6)$$

The material constants F, β and K are obtained from balanced loop data, whilst d is found from unbalanced loop data.

Equation (6) is the latest in the development of a series of frequency modified approaches. For the data obtained on a 1CrMoV steel tested at 565°C /70/, agreement with Equation (6) was reasonably good, though several of the data did fall outside the x2 life scatterband (Fig. 19a). Further, for type 304 stainless steel, data obtained using a wide variety of test waveforms have successfully been correlated by Coffin /77/, (Fig. 19b). Thus, the frequency separation method, though phenomenological in its approach, appears capable of numerically predicting lives reasonably well.

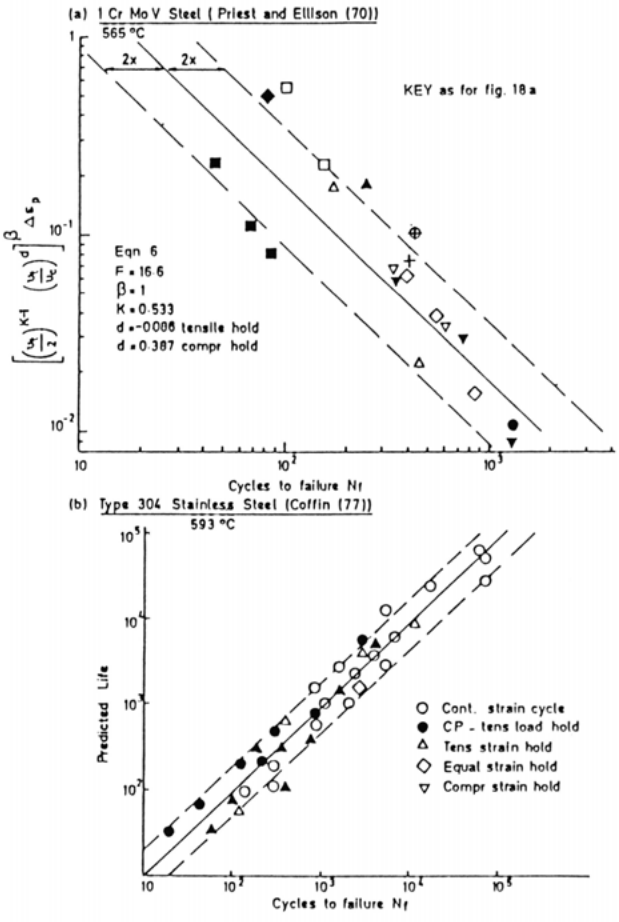

Fig. 19. Frequency separation approach

The major drawback of this approach is in the number of numerical coefficients necessary to evaluate equations (3), (4) and (6). Indeed, cyclic-hold test data are required for the implementation of equation (6). Further, as with the linear life fraction method, the lack of fundamental mechanistic understanding in the derivation of this method means its success in life prediction is likely to be material dependent.

It is worth noting that a further extension of Coffin's approach has been made by Ostergren /36, 79/ in which stress as well as strain range was used to describe failures under fatigue-creep conditions. Ostergren consid ed that damage could be characterised by

a tensile hysteresis energy term, any dependence on life due to the shape of the imposed waveform also being taken into account. Unfortunately, large errors were obtained when trying to use this method with 1CrMoV steel data /70/, though Ostergren himself obtained better agreement with 316 stainless steel test data /79/.

3.3. *Strainrange Partitioning*

This approach was introduced by Manson and co-workers /80-85/ in an attempt to take account of the damage caused by different types of strain. It was proposed that the inelastic strain accumulated during one high temperature cycle could be partitioned into four possible kinds of strain range, depending on the direction of straining (tension or compression) and the type of inelastic strain accumulated (creep or time-independent plasticity). Thus, any reversed inelastic strain range could be partitioned into a combination of the following components: $\Delta\epsilon_{pp}$, $\Delta\epsilon_{cp}$, $\Delta\epsilon_{pc}$ and $\Delta\epsilon_{cc}$. Here, for example, $\Delta\epsilon_{cp}$ represents a tensile creep strain reversed by compressive plastic strain.

Figure 20 shows idealised hysteresis loops for the four generic types of strain ranges. For the pure generic strain range types, the basic life relationships follow the Manson-Coffin form:

$$\begin{aligned} N_{pp} &= A\,(\Delta\epsilon_{pp})^{\alpha_1} \\ N_{cp} &= A\,(\Delta\epsilon_{cp})^{\alpha_2} \\ N_{pc} &= A\,(\Delta\epsilon_{pc})^{\alpha_3} \\ N_{cc} &= A\,(\Delta\epsilon_{cc})^{\alpha_4} \end{aligned} \qquad (7)$$

where the coefficients A and exponents α are experimentally determined material constants. Clearly, in practice $\Delta\epsilon_{cp}$ and $\Delta\epsilon_{pc}$ cannot co-exist in the same loop.

For actual cycles, a cumulative damage rule is required to account for the different types of strain occurring. Assuming that the inelastic strain in the loop is $\Delta\epsilon_{in}$, the component fractions are:

$$\begin{aligned} F_{pp} &= \frac{\Delta\epsilon_{pp}}{\Delta\epsilon_{in}}, \qquad F_{cp} = \frac{\Delta\epsilon_{cp}}{\Delta\epsilon_{in}}, \\ F_{cc} &= \frac{\Delta\epsilon_{cc}}{\Delta\epsilon_{in}}, \qquad F_{pc} = \frac{\Delta\epsilon_{pc}}{\Delta\epsilon_{in}}. \end{aligned} \qquad (8)$$

The predicted lives, N_{fpred}, can then be obtained

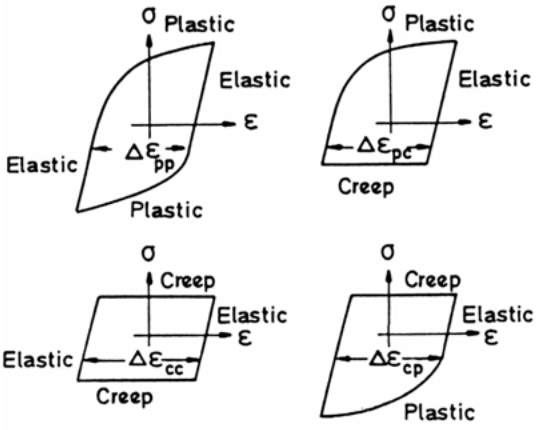

(a) Idealized hysteresis loops for the four basic types of inelastic strain range

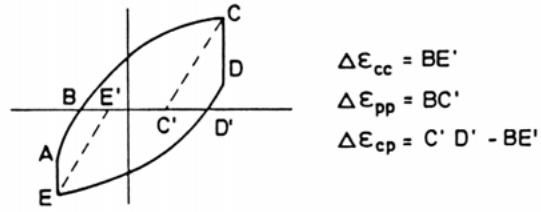

(b) Hysteresis loop containing $\Delta\epsilon_{pp}, \Delta\epsilon_{cc}, \Delta\epsilon_{cp}$

Fig. 20. Strainrange partitioned hysteresis loops /40/

from the following interaction damage rule:

$$\frac{1}{N_{fpred}} = \frac{F_{pp}}{N_{pp}} + \frac{F_{cc}}{N_{cc}} + \frac{F_{cp}}{N_{cp}}\ [\text{or}\ \frac{F_{pc}}{N_{pc}}] \qquad (9)$$

Partitioned strain ranges for various alloys are shown in Fig. 21. The representation clearly indicates that the 1CrMoV steel, and both 304 and 316 stainless steels, are weakest for cycles including tensile hold periods. For the 2¼Cr-1Mo and nickel base alloys Rene 80 /40/ and Waspalloy /86/ it appears that compressive hold periods are more damaging.

Predictions using the SRP approach for a 1CrMoV steel and 316 stainless steel are shown in Fig. 22. Whilst for the 316 steel /87/, predictions appear to be reasonably good, for the 1CrMoV steel the SRP approach seems inadequate in describing cyclic-hold tests with either very short or very long tensile dwells /70/. In this latter case Priest and Ellison /70/ showed that for 1CrMoV steel during short hold periods, large

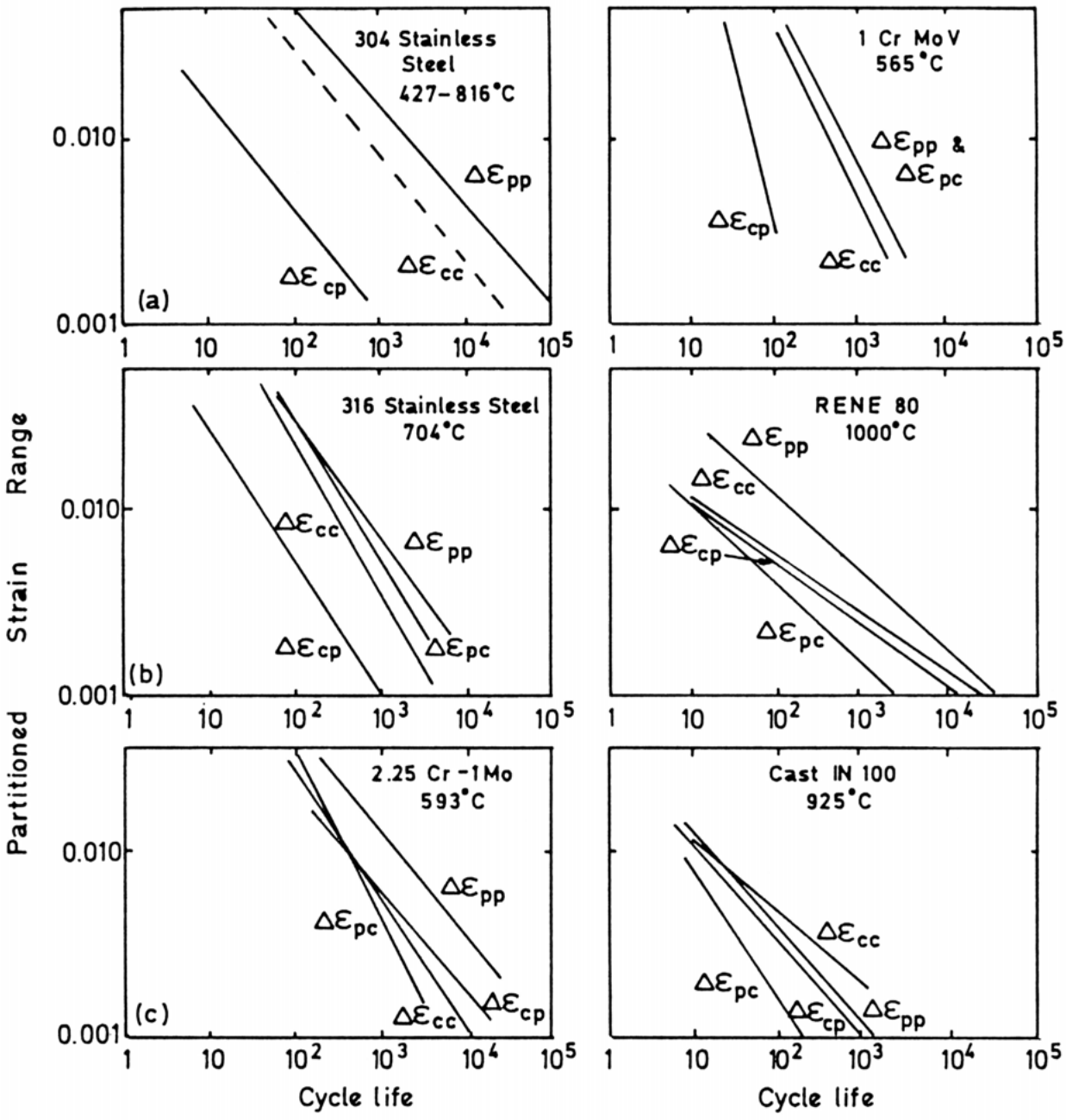

Fig. 21. Combined strain range partitioning relations for various alloys /40,88,92,93/

cp strain components are accumulated very rapidly, only a small part of the strain accrued during this time being attributable to creep damage. SRP, however, considers all the cp strain components to be equally damaging, and the resulting predictions are conservative. As the duration of the hold periods is increased, increasingly non-conservative predictions result, clearly indicating that SRP cannot model time dependent effects in its standard form.

Attempts have been made to overcome these problems with SRP by accounting for hold time and strain rate effects /88, 52/. Further developments of the SRP approach have included ductility normalisation /83/ and its application to multiaxial fatigue-creep /89, 90/. More recently, an approach which applies SRP to total strain ranges has been examined /91/.

Thus, much data have been presented which apply the SRP approach to a range of materials, the approach yielding conflicting evidence for /98, 92-94/ and against the method /70, 95, 96/. Problems with the SRP ap-

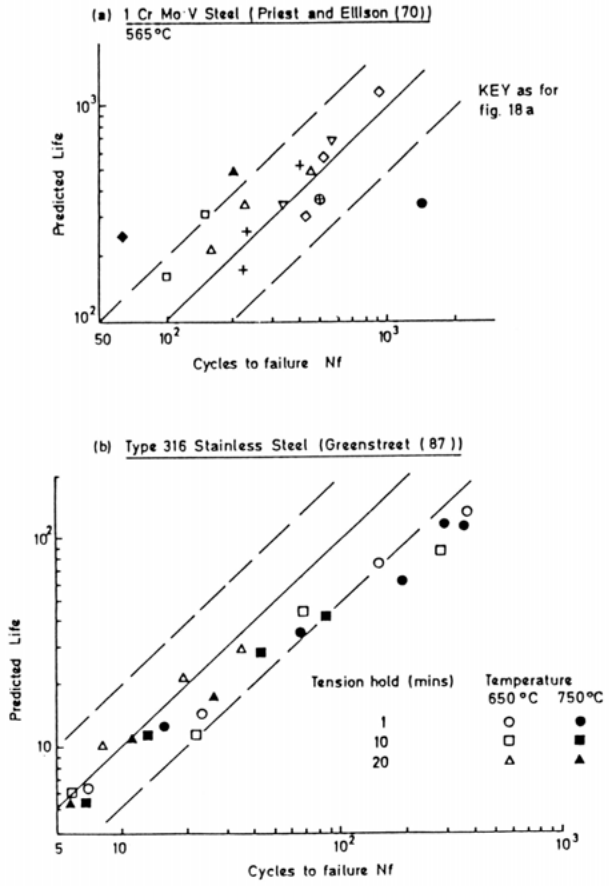

Fig. 22. Strainrange partitioning approach

proach stem from its phenomenological nature and the fact that relatively complex cyclic-hold tests must be performed to generate the baseline data. Once these data have been obtained, however, the approach is simple to apply, though its accuracy under extrapolated conditions of hold time or reduced strain range remains questionable.

3.4. Damage Rate

The strain based damage rate approach developed by Majumdar and Maiya /78, 97-99/ also takes account of the rate at which fatigue or creep damage is accumulated. In its simplest form /97, 98/ failure was said to occur when pre-existing cracks of length a_o grew to a critical length a_f, one or more of these cracks linking to form a macrocrack. The growth of each microcrack was assumed to be governed by the equations:

$$\frac{da}{dt} = a\left[\frac{T}{C}\right]\left[\epsilon_p\right]^m\left[\dot{\epsilon}_p\right]^K \qquad (10)$$

where T, C, m and K are material parameters which are functions of temperature, environment and the metallurgical state of the material. T and C are included to account for differences that can occur in growth rates under tension and compression; for data on 304 stainless steel, Majumdar and Maiya /97/ used T/C = 4.

For continuous cycling over a plastic strain range $\Delta\epsilon_p$ at constant plastic strain rate $\dot{\epsilon}_p$, Equation (10) can be integrated to give the cycles to failure, viz:

$$N_f = \left[\frac{(m+1)}{4A}\right]\left[\frac{\Delta\epsilon_p}{2}\right]^{-(m+1)}\left[\dot{\epsilon}_p\right]^{1-K} \qquad (11)$$

where

$$A = \frac{(T+C)}{2}\ln(a_f/a_o)$$

An extension of the original approach was subsequently proposed by Majumdar and Maiya /78, 99/ in which damage was considered to be made up of crack damage (fatigue) and cavity damage (creep) which accumulate independently. The rate of fatigue damage is still given by Equation (10) but, in addition, cavity growth rates are assumed to be described by:

$$\frac{1}{c}\frac{dc}{dt} = \left(\frac{G}{-G}\right)\left|\epsilon_p\right|^m\left|\dot{\epsilon}_p\right|^{K_c} \qquad (12)$$

where c is the cavity size at time t, and G and K_C are material parameters. Note that parameter G is given the appropriate sign for tensile or compressive stress regimes. Final failure is calculated as the reciprocal of the sum of the crack and cavity damage.

More recently, an interactive damage equation has been proposed by Majumdar and Maiya /100/ in which the crack growth rate is assumed to be increased by the presence of cavities. The cracks and cavities are assumed to grow according to the following interactive damage equations:

$$\frac{1}{a}\frac{da}{dt} = \left(\frac{T}{C}\right)\left[1 + \alpha\ln\frac{c}{c_0}\right]\left|\epsilon_p\right|^m\left|\dot{\epsilon}_p\right|^K \qquad (13)$$

$$\frac{1}{c}\frac{dc}{dt} = \left(\frac{G}{-G}\right)\left|\epsilon_p\right|^m\left|\dot{\epsilon}_p\right|^{K_c} \qquad (14)$$

where the material parameters T, C, m, K, G, K_C are functions of temperature, environment, and microstructure of the material. Similarly, α is a material parameter which is zero for continuous cycling or loadings with compressive imbalance, when cavities are assumed not to initiate.

Since it has previously been shown that fatigue and creep damage accumulate independently for 1CrMoV

steel tested at 565°C /11/, the non-interactive damage equations were used by Priest and Ellison /70/ to correlate these material data, (Fig. 23a). It can be seen that the correlation is extremely good except for the one short hold time result. Other data for type 304 stainless steel for different temperatures and varying hold times showed similar good agreement, (Fig. 23b), Majumdar and Maiya /97/ also obtaining good correlation for type 316 steel, Incoloy 800 and 2¼Cr-1Mo steel.

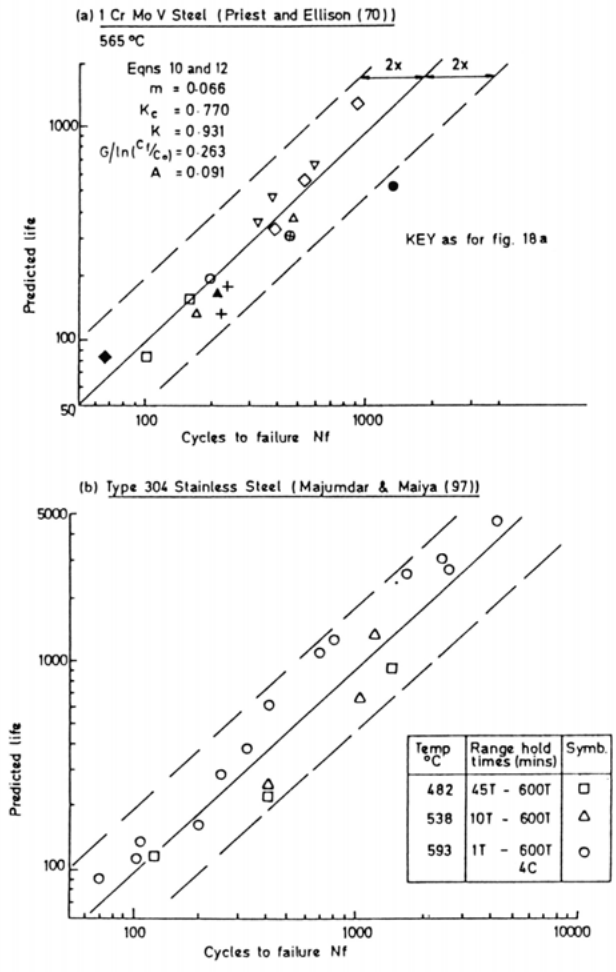

Fig. 23. Damage rate approach

The approach is attractive in that it can model the "healing" effect of a compressive dwell on a previous tensile dwell. However, values for many coefficients in the lifetime equations must be obtained before the method can be used. Indeed, evaluation of some of these coefficients depends on the results of complex cyclic-hold tests, so their generation is both expensive and time-consuming. Nevertheless, although only few materials have been used to validate this prediction technique, its simplistic mechanistic basis is attractive and the good results indicate that the method is promising as a universal approach; recent attempts to present the various damage terms in a graphical form also add to the appeal of this method /70/.

3.5. Ductility Exhaustion

Following cyclic-hold bend tests on a 2¼Cr-1Mo steel at 600°C, Edmunds and White /19/ attempted lifetime predictions based on the assumption that specimen failure occurred when the accumulated creep relaxation strain equalled the rupture ductility of the material. This method was shown to underestimate endurance substantially. However, some years later, Priest and Ellison /101/ modified this approach by taking account of the strain rate dependence of the accumulated creep strain. These authors subsequently devised a "ductility exhaustion" approach to life prediction which yielded extremely good results for a range of tests performed on a 1CrMoV steel tested at 565°C.

Essentially, it was shown that by partitioning cyclic-hold hysteresis loops into "true" creep and plasticity components using transition strain rate concepts /52/, creep dominated endurances could be predicted using the simple equation /101/:

$$N_c \, \Delta\epsilon_{ct} = D_c \qquad (15)$$

where $\Delta\epsilon_{ct}$ is the true tensile creep strain component at half-life (i.e. that accumulated at a rate below the transition value used to signify the onset of internal intergranular creep damage), D_c the lower bound creep ductility and N_c the lifetime for creep dominated failures. Similarly, fatigue dominated endurances were approximated by:

$$N_p \Delta\epsilon_p = D_p \qquad (16)$$

where $\Delta\epsilon_p$ is the plastic strain component at half life (i.e. that not associated with any grain boundary damage), D_p the fatigue ductility obtained from pure fatigue test data, and N_p the fatigue dominated lifetime.

Metallographic evidence /11/ revealed that for the 1CrMoV steel data obtained by Priest and Ellison, creep and fatigue damage accumulated essentially independently of one another. Thus, for this situation of negligible fatigue-creep interaction, it was postulated

that both creep and fatigue mechanisms competed to cause failure. The mechanism that reached its critical ductility in the least number of cycles was therefore taken as that determining both the specimen lifetime and the predominant mode of failure, the following damage law being used:

$$\frac{\Delta\epsilon_{ct}}{D_c} \quad \text{or} \quad \frac{\Delta\epsilon_p}{D_p} = \frac{1}{N_{pred}} \tag{17}$$

Predictions obtained using equation (17) are shown for the 1CrMoV steel in Fig. 24. With only one exception numerical predictions are within two times the observed lives, these predictions also being predominantly conservative. In addition, excellent correlation was observed between predicted and observed dominant failure modes /101/.

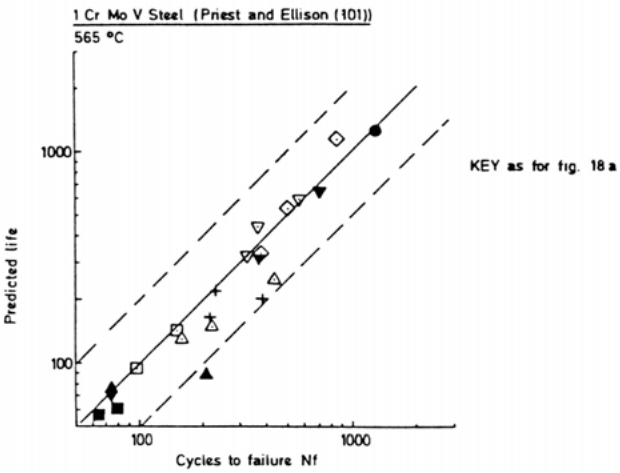

Fig. 24. Ductility exhaustion approach

Later work by Ellison and co-workers /102/ also applied the ductility exhaustion technique to both isothermal and thermal-mechanical test data obtained on the austenitic type 316 steel. Although fewer data were available from tests on this material, an interaction between the creep and fatigue damage mechanisms was identified for certain combinations of strain range, temperature and hold time. From the 1CrMoV steel data /11/, failure was generally seen to occur as the result of one dominant mechanism. Under these conditions the "competitive" equation (17) is best used for predictions. However, to cater for interactive conditions, the more pessimistic "additive" damage equation:

$$\frac{\Delta\epsilon_{ct}}{D_c} + \frac{\Delta\epsilon_p}{D_p} = \frac{1}{N_{pred}} \tag{18}$$

was used with the ductility exhaustion approach. This equation was found to give excellent predictions for the isothermal and non-isothermal tests applied to the 316 steel /102/.

Micromechanistic support for the use of equation (15) has been given by Miller *et al.* /103/. These workers developed an analytical model for predicting the fatigue-creep endurance of constant strain dwell tests through the application of cavity growth mechanisms to the stress relaxation periods. Three major cavity growth mechanisms were considered /103/:

1. deformation growth /48/;
2. unconstrained grain boundary diffusion growth /49, 50/;
3. geometric constrained growth /51/.

Constitutive endurance equations were subsequently described for these growth mechanisms, and maps constructed illustrating the region where each specific mechanism dominated.

For tensile dwell tests performed on 1CrMoV steel at 565°C, Miller *et al.* /103/ predicted that constrained cavity growth mechanisms would be operative during the major part of the dwell period. Under these conditions the endurance equation was found to be:

$$N_f = \frac{\pi\lambda}{6d} \cdot \frac{1}{\Delta\epsilon_{ct}} \tag{19}$$

where d is the grain size, λ the cavity spacing and $\Delta\epsilon_{ct} = (\sigma_1 - \sigma_h)/E$ where σ_1 is the stress after 1 minute of the dwell period and σ_h the stress at the end of the dwell period. Comparing this equation with equation (15) it can be seen that $D_c = \pi\lambda/6d$ which is in agreement with the work of Dyson and Loveday /104/. Using $\lambda = 3\mu m$ /103/ and the value of d measured for the 1CrMoV steel /101/ gave a value for D_c of 6.8×10^{-2}, which compares well with the lower bound ductility measured by Priest and Ellison (Fig. 25). This therefore provides some mechanistic basis for the use of the ductility exhaustion technique for predicting failure in the creep dominated regime. It will be noted, however, that equation (19) relies on the knowledge of λ and that this is a parameter not easily determined. In addition, the value of $\Delta\epsilon_{ct}$ is not determined on any mechanistic basis but simply by a division of strain rates into transgranular and intergranular processes.

Constitutive equations for use in predicting the

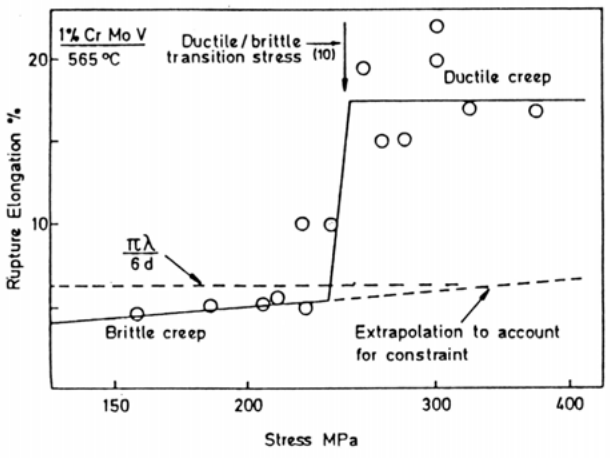

Fig. 25. Static creep rupture elongation vs. stress for 1CrMoV steel together with the predicted minimum creep ductility using $\pi\lambda/6d$ /103/

creep dominated failure of specimens during slow-fast cycling have also been developed by Miller /105/ and Beere /106/. In slow-fast cycling the ductility exhaustion approach is particularly easy to apply, since the tensile strain rate is constant in these tests, whereas it varies during dwell period tests. Miller /35/ showed that by using the ductility exhaustion approach given by:

$$N_f = \frac{D_c}{\Delta\epsilon_p} \tag{20}$$

where D_c is the creep ductility at the tensile strain rate, and $\Delta\epsilon_p$ the plastic strain range, good agreement could be obtained between observed and predicted endurance for slow-fast cycling in 20%Cr/25%Ni/Nb stainless steel, as shown in Fig. 9.

A further development of the ductility exhaustion technique has been attempted by Hales /107/ following tests on a 316 stainless steel. A more generalised description of the variation in monotonic ductility as a function of strain rate was proposed /107/, since the transition from low to high ductility was more gradual for the 316 steel than that described by Priest and Ellison /101/ for the 1CrMoV steel. The method is similar to that described by Miller *et al.* /103/ except that actual creep rupture data were used as the basis for fatigue-creep predictions rather than detailed models for defect growth.

The experimental ductility data for the Austenitic steel were described by three discontinuous linear functions /107/ (Fig. 26) viz:

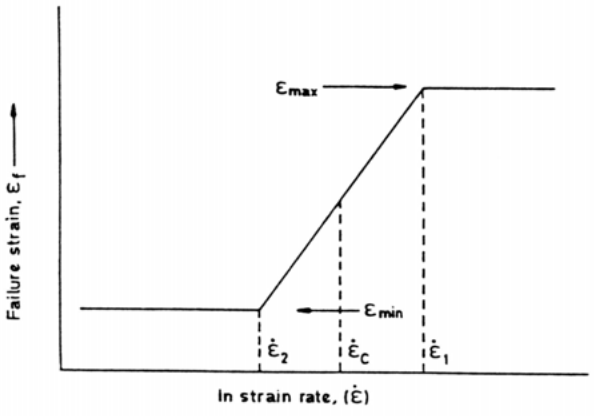

Fig. 26. A schematic presentation of the variation of failure strain (ductility) with strain rate /107/

$$\dot{\epsilon} > \dot{\epsilon}_1 \qquad \epsilon_f = \epsilon_{max} \tag{21a}$$

$$\dot{\epsilon}_1 > \dot{\epsilon} > \dot{\epsilon}_2 \qquad \epsilon_f = A \ln(\dot{\epsilon}) + B \tag{21b}$$

$$\dot{\epsilon}_2 > \dot{\epsilon} \qquad \epsilon_f = \epsilon_{min} \tag{21c}$$

where the symbols are as defined in the figure. Thus, during a hold period, as the strain rate decreases the damage contributions from each of three regimes are summed. However, it should be noted that for long dwell periods, the contribution from equations 21(a) and 21(b) will be very small compared with 21(c), and thus this approach converges to the previous models. Hales went on to take account of the healing effect on cavities due to any cyclic compressive excursions, and an expression for the nett damage per cycle was obtained. Using this formalism, good predictions for a limited range of creep dominated cyclic-hold tests performed on a 316 steel at 600°C were obtained (Fig. 27).

Hales /31/ has recently applied this version of ductility exhaustion to ½CrMoV steel data obtained at 550°C. The data were for two cycle types, the normal laboratory cycle with a tensile dwell at peak strain and a cycle in which the dwell period was introduced at zero strain in the tensile part of the cycle. The comparison between predicted and observed endurance is given in Fig. 28. Good agreement was obtained at strain ranges less than 1% (where creep dominated failures were dominant). However, at higher strain ranges (between 1 and 2%), the observed endurance was a factor of 1.5 to 3 worse than predicted by a creep-damage summation. This is not surprising since a fatigue-creep interaction mechanism dominated these failures /7/. This underlines the need to understand

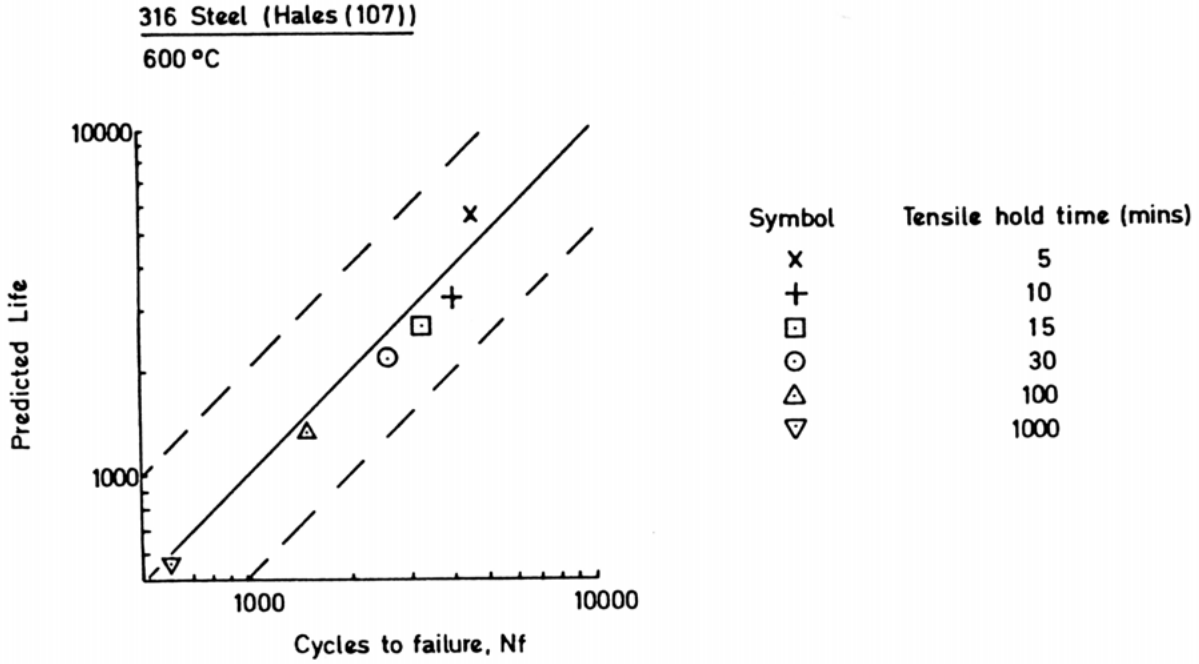

Fig. 27. Ductility exhaustion approach

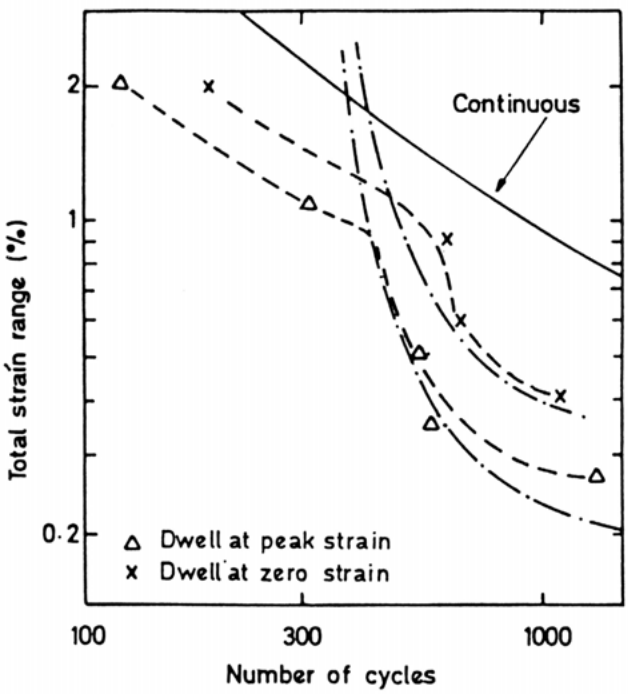

Fig. 28. A plot of endurance as a function of strain range for two test conditions
------ experimental behaviour
——— endurance calculated by strain summation /31/

the dominant failure mechanism if reliable predictions are to be obtained.

The ductility exhaustion method has thus been successfully used by a number of workers using both ferritic /101, 46, 31/ and austenitic steels /105, 102, 107/. Despite this success, and the simplicity of the ductility exhaustion technique, there are a number of difficulties in using the method. Not least of these is knowing, especially for hold period tests, which part of the creep strain accumulated during the dwells corresponds to "true" creep damage, and which is due to relatively undamaging "anelastic" effects. Although methods have been devised from both experimental /52, 103/ and analytical considerations /101, 102/ it must be acknowledged that these are open to error. The alternative approach /107/ of integrating all damage contributions during the hold periods appears, superficially, to avoid such problems. However, the strain rate (or rates) over which there is a transition from low to high ductility has been shown (section 2.5) to be affected both by macroscopic constraint /52, 46/ i.e. strain limited testing, and triaxial effects /53/. For typical service situations therefore, designers would not know where the transition actually occurs. In addition, it should be noted that there are a number of different ways in which ductility can be measured, viz: reduction of area, elongation or $\dot{\epsilon}t_r$. However, a lower bound value for conservative predictions is given by $\dot{\epsilon}t_r$ as shown in Fig. 13.

It should be noted that the "healing" effect of

compressive dwells on prior tensile dwells can be accommodated by the ductility exhaustion technique. From equation (15), for example, the term $\Delta\epsilon_{ct}$ is taken to be the net tensile creep strain increment (i.e. $\Delta\epsilon_{c_{tension}} - \Delta\epsilon_{c_{compression}}$) accumulated per cycle; this term reduces to zero if $\Delta\epsilon_{c_{compression}} > \Delta\epsilon_{c_{tension}}$. Thus, compression only hold period test predictions would be obtained through the use of an equation such as equation (16). Note that with compressive holds, equation (16) would give lifetimes slightly smaller than those observed for pure fatigue tests, since $\Delta\epsilon_p$ includes the strain accumulated during both the fatigue cycles *and* from the rapid relaxation part of the dwells. Although this is in agreement with most observed behaviour (Fig. 3) it must be acknowledged that it is likely that the method could not predict the very damaging compressive hold data observed for, say, nickel base superalloys.

To summarise, the ductility exhaustion method has been successfully used by a number of workers /101, 102, 105, 107, 31, 46/. The method is attractive since it is simple to use and has some mechanistic basis /103/, making its use under extrapolated conditions more certain. There are difficulties in quantifying the strain/damage contributions, however.

3.6. *Crack Propagation*

The work of Tomkins and Wareing /108-111/ has led to a model for fatigue-creep interactions which assumes that all the specimen endurance is taken up in crack propagation. In his model for fatigue crack propagation, Tomkins /108/ assumed that the extent of propagation was given by the amount of decohesion at the crack tip. The plastic zone size ahead of the crack was used to model the crack propagation rate, this zone size D_z being given by:

$$D_z = \sqrt{2}\,(\sec\frac{\pi\sigma}{2\sigma_u} - 1)a \qquad (22)$$

where σ_u is the ultimate stress and a the crack length. Under the applied stress σ Tomkins approximated the amount of new crack growth by $\Delta\epsilon_p D_z$ and used the equation

$$\frac{da}{dN} = \frac{\Delta\epsilon_p D_z}{\sqrt{2}} \qquad (23)$$

to describe the rate of crack propagation. By substituting for D_z in the above equation and integrating, the lifetime under pure fatigue situations was described by the equation /108/:

$$N_f = \ln(\frac{a_f}{a_o})/\Delta\epsilon_p\,[\sec\frac{\pi\sigma_{max}}{2\sigma_u} - 1] \qquad (24)$$

where σ_{max} is peak tensile stress, and a_o and a_f are the initial and final crack lengths, respectively. Equation (24) was subsequently treated by Wareing /20/ as an upper bound on endurance, since it described pure fatigue conditions only.

A lower bound case was then considered in which the plastic zone size became effectively infinite. For this case the endurance relationship becomes:

$$\Delta\epsilon_p N_f \doteq a_f/W \qquad (25)$$

where W is the width of the specimen.

Under simultaneous cyclic-hold test conditions, the creep damage formed during constant strain hold periods increases the plastic zone size associated with a surface fatigue crack /111/ until it extends it across the specimen width. It was argued that equation (25) describes the endurance under these conditions. For cycles containing varying periods of tensile relaxation, specimen lifetimes should be between the upper and lower bounds described by equations (24) and (25), respectively. Figure 29 shows that equations (24) and (25) do indeed bound the data from tests on a range of steels /20, 22, 70, 112, 74, 21/.

Recent work by Wareing and co-workers /26, 113, 114/ has considered more closely the interactive effect of internal grain boundary cracks occurring ahead of surface fatigue cracks. Using the model that, once initiated, surface crack growth takes place in the three phases shown schematically in Figure 30, Tomkins and Wareing /113/ reasoned that the increase in crack growth rate during phase II was due to the attainment of cavity linkage at the crack tip. This causes the unzipping of cavitated material by the crack displacement field instead of through a continuous controlled crack advance mechanism. The crack tip condition was given by:

$$\delta/2 = \lambda - p = \text{ligament length to be ruptured} \qquad (26)$$

where δ is the fatigue crack tip opening displacement, p is the cavity diameter and λ the intercavity spacing.

Lloyd and Wareing /115/ and Michel and Smith /116/ have also related the acceleration in crack growth rates during load controlled interactive growth to the development of a critical intergranular cavity size and spacing, related to carbide spacing. However, other workers /117/ have been unable to determine any

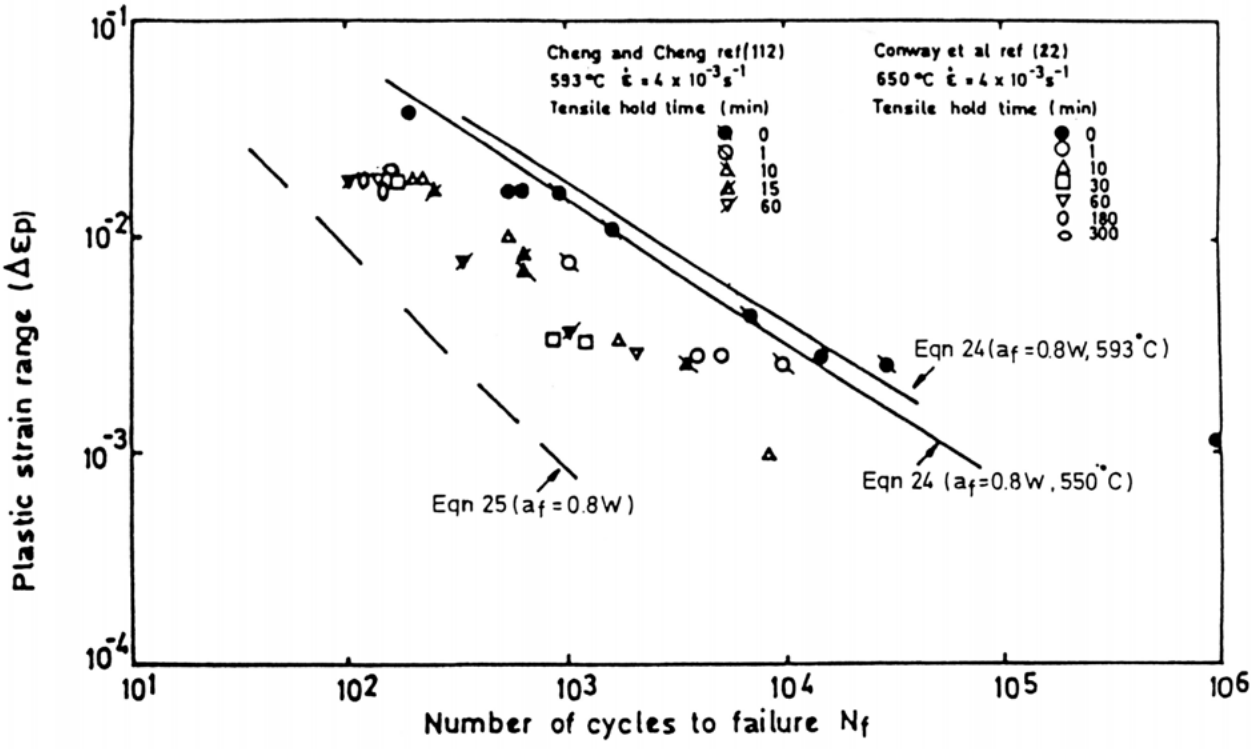

(a)

EFFECT OF TENSILE HOLD PERIOD ON 304 STAINLESS STEEL (20)

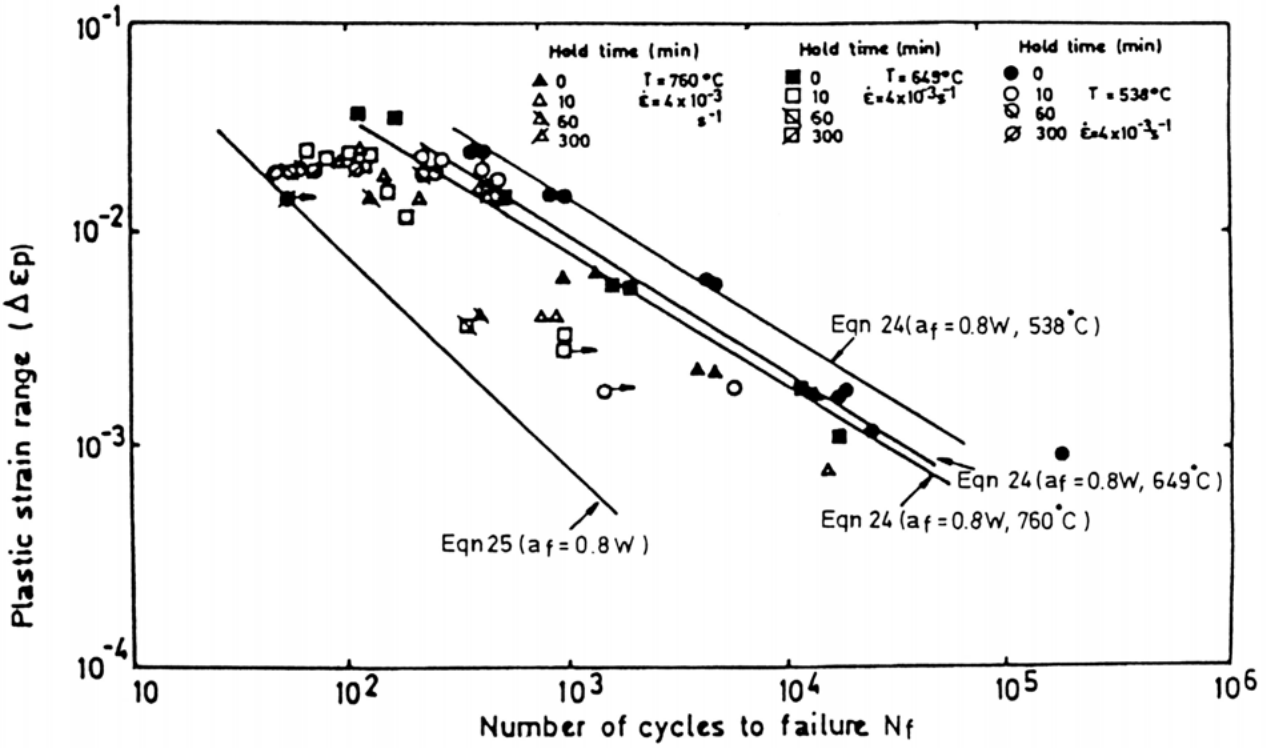

(b)

EFFECT OF TENSILE HOLD PERIOD ON INCOLOY 800 (74,20)

Fig. 29. Crack propagation bounding predictions

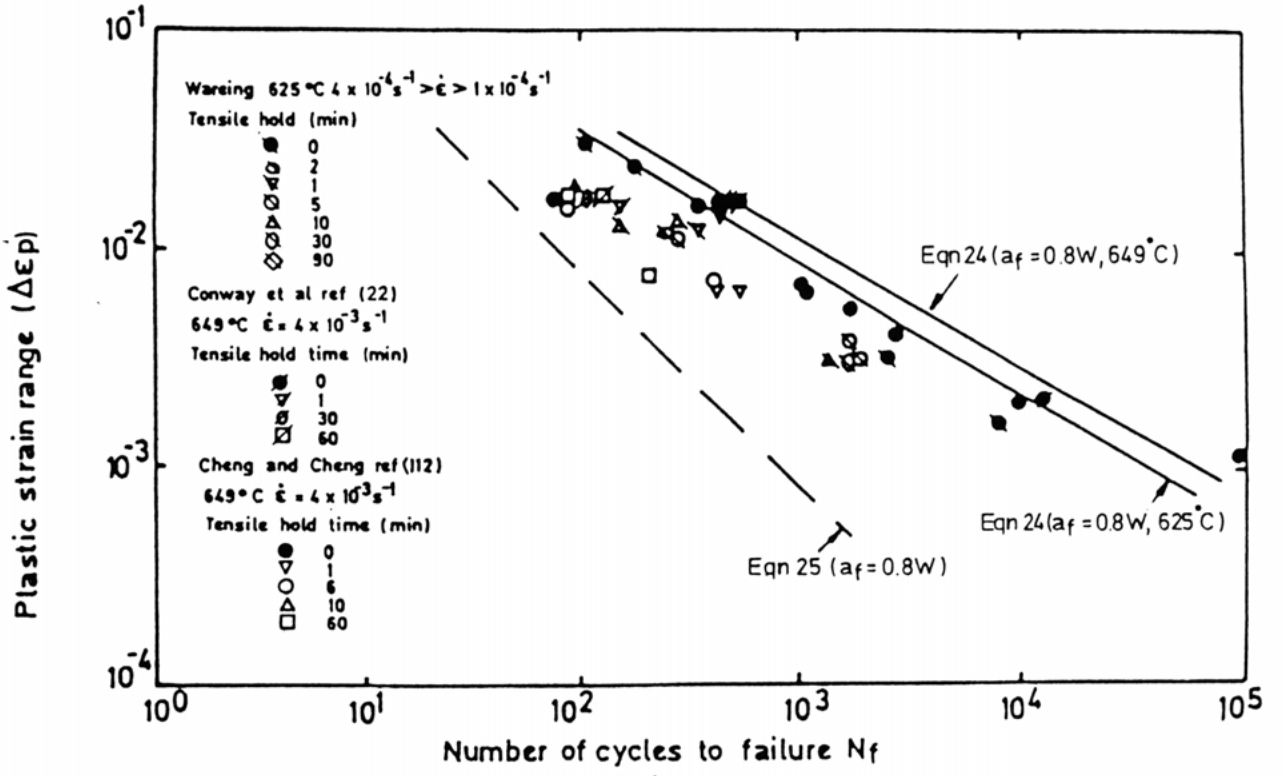

(c)

EFFECT OF TENSILE HOLD PERIOD ON 316 STAINLESS STEEL (20)

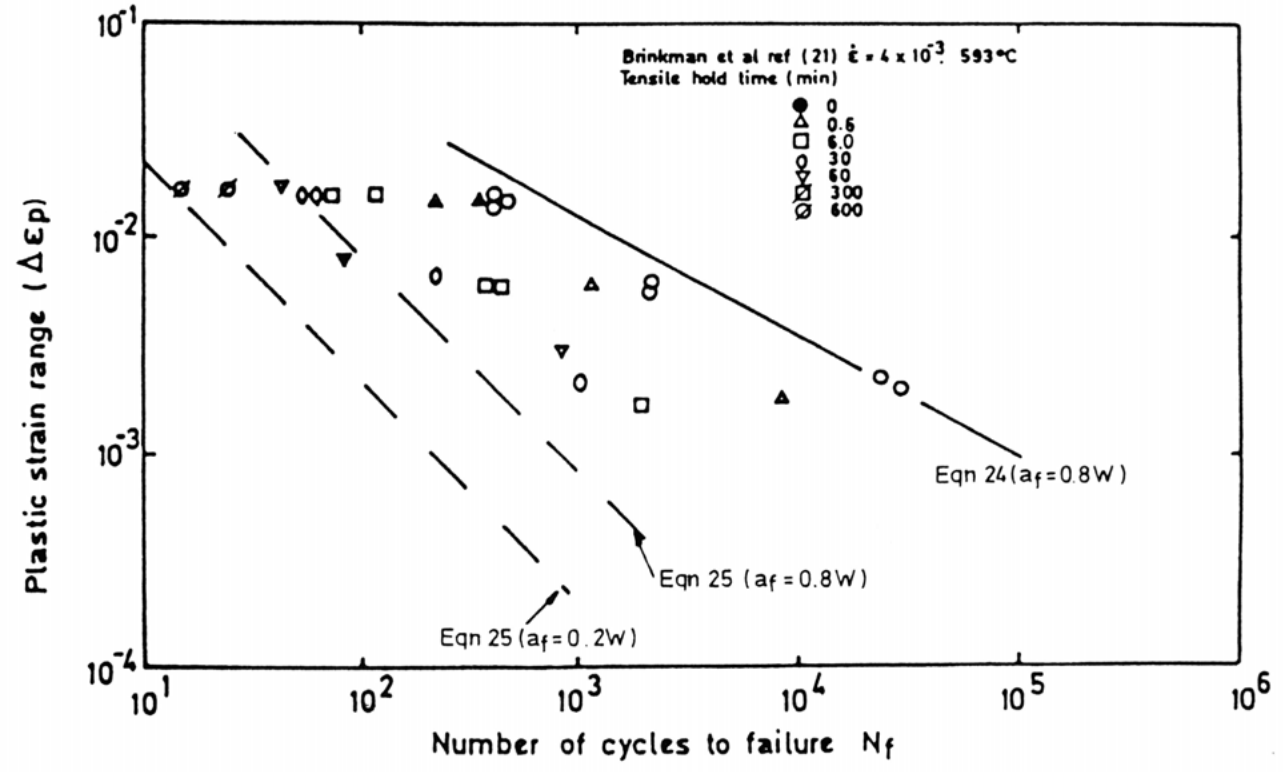

(d)

EFFECT OF TENSILE HOLD PERIOD ON 316 STAINLESS STEEL (20)

Fig. 29. (cont)

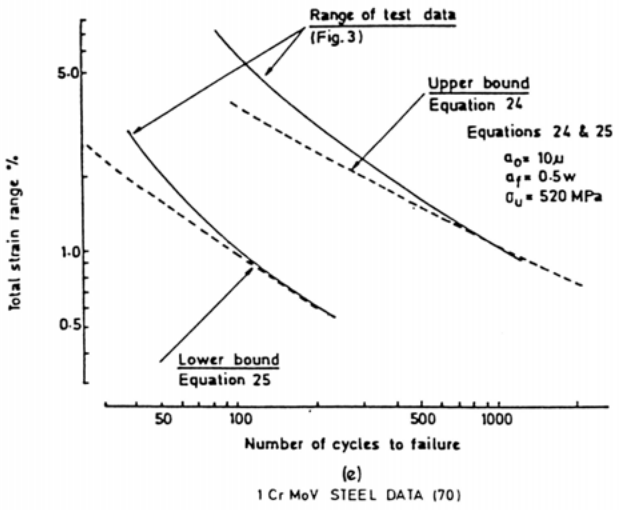

Fig. 29. (cont)

significant influence of carbide particles on cavity formation, since interactive growth has been observed in both unaged and long term aged steels. Also, in contrast to the work of Lloyd and Wareing /115/ and Michel and Smith /116/, a retardation in fatigue-creep crack growth rate has been found in 20% cold worked 316 steel following ageing /118/.

The endurance of a specimen failing by the interactive growth mechanism was thought essentially to be that given by the cycles to initiation plus Phase 1 fatigue crack growth, since Phases II and III occur so rapidly. Thus, assuming that fatigue-creep endurance is devoted entirely to fatigue crack propagation, endurance values were obtained from equation (24). A value for a_o was taken to be some representative measured value (typically 10 μm) whereas a_f was obtained from the equation.

$$\delta_{1/2} = \lambda - p = \ln\sec\left(\frac{\pi\sigma_{max}}{2\sigma_u}\right)\left[\frac{2\sigma_u}{E} + \frac{2\Delta\epsilon_p}{1+\beta}\right]a_f \qquad (27)$$

where β is the cyclic work-hardening exponent.

Using this predictive method, Wareing and co-workers obtained good lifetime predictions for different casts of 316 steel tested under cyclic-hold conditions and 20%Cr-25%Ni/Nb steel tested using slow-fast cycling /33/, Fig. 31.

The main drawback of this model for fatigue-creep interactions is the need to determine the cavity spacing, λ-p, since some degree of subjectivity is involved in its evaluation. In addition, one value of λ-p is insufficient since this will vary with the testing conditions.

Nevertheless, for design purposes in particular, there may be merit in using the lower-bounding technique initially proposed by Wareing and co-workers through equation (25). Although not as 'sophisticated' as some models, uncertainties in the more complex methods, such as the identification of relevant damage contributions, make a lower bound approach very attractive. However, the approach adopted by equation (25) is too simplistic, since it can not accommodate changes in material properties. For example, if the ductility is substantially reduced due to irradiation or microstructural effects then lifetimes could be obtained which are below the lower bound predicted by equation (25). It should be noted, however, that ductility exhaustion can accommodate such changes in material behaviour due to in-service exposure.

The next section deals with design rules, and proposes some improvements that can be made to existing codes as a result of the various life prediction techniques outlined above.

4. DISCUSSION

4.1. Background

From the foregoing sections, it has been shown that a number of different prediction techniques have been evolved, each primarily to account for a particular set of material response conditions. Thus, whilst each technique can be used to cater for any one set of conditions, such as environmental effects, none of the available techniques can apriori predict the behaviour of a range of materials tested under a range of testing conditions. It must be admitted that the prospect of obtaining such a general approach is very remote. However, much work has been performed on steels used in power plant applications. Indeed, current design codes have largely been formulated around steels data, and in this section, attention is focussed on these materials. Of most relevance in this context is the adaptation of the linear life fraction rule (section 3.1) to form the basis of ASME Code Case N-47 /5/.

4.2. Design Codes

For ASME Code Case N-47, the linear life fraction equation can be modified to give a limit for the allowable damage D. Generally, Code Case N-47, is given by:

$$\Sigma\frac{N}{N_d} + \Sigma\frac{T}{T_{d'}} \leqslant \begin{matrix}\text{D for inelastic route}\\ \text{1 for elastic route}\end{matrix} \qquad (28)$$

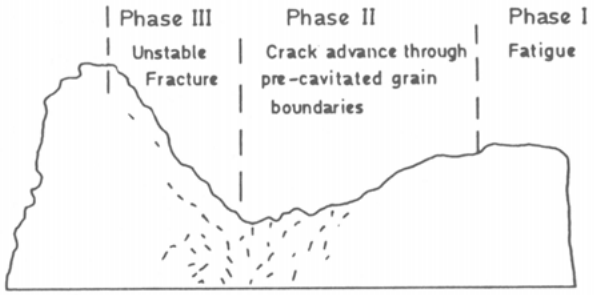

Fig. 30 (a) Schematic representation of the three phases of crack growth which occur during fatigue-creep failure /113/

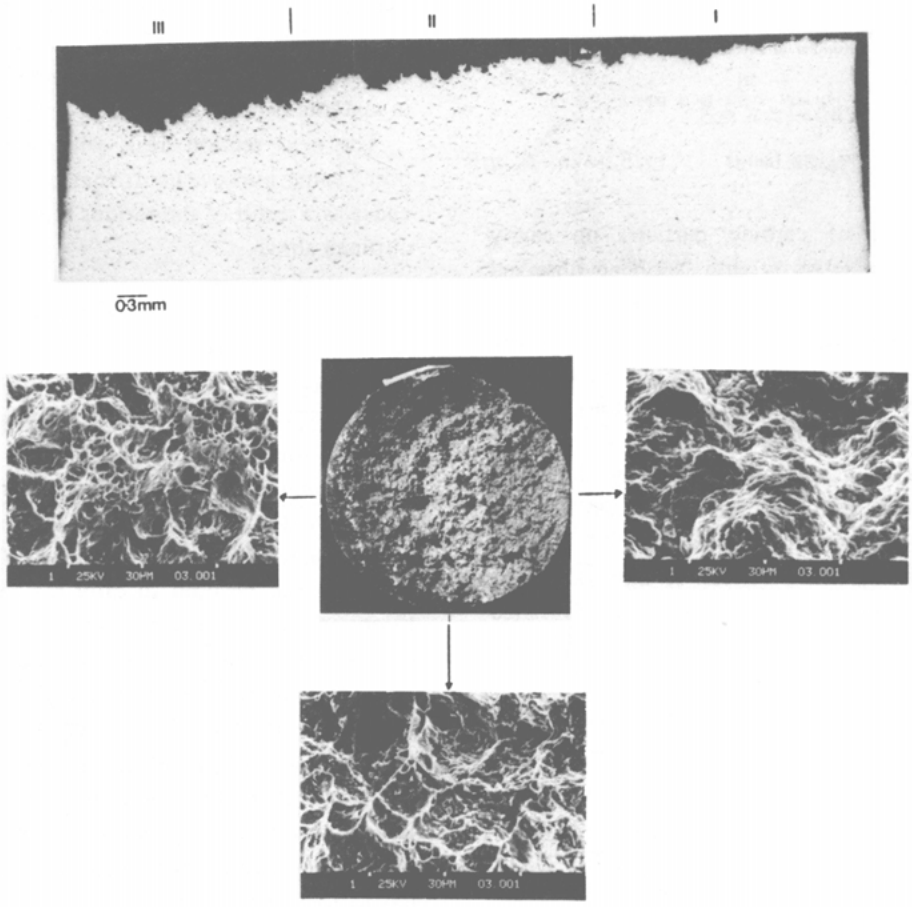

Fig. 30. (b) Example of three phase crack growth in fatigue-creep interaction /35/

where N is the number of cycles of the loading condition, N_d the number of allowable cycles of the loading condition at the maximum temperature during the cycle, T the duration of the loading condition, and T'_d the time to rupture at a stress given by the applied stress divided by 0.9 for most steels. The terms 'elastic' and 'inelastic' refer to the numerical techniques used to quantify stress/strain responses as a result of any desired loading requirements.

4.2.1. Inelastic route

In order to evaluate N_d using the "inelastic" route, continuous cycle design curves, incorporated in N-47, are used (Fig. 32). These design curves implicitly include factors of safety (i.e. 2 on strain or 20 on cycles) for conservatism.

To evaluate the creep damage term, the life fraction integral $\int dt/T_d'$ is evaluated per cycle using minimum

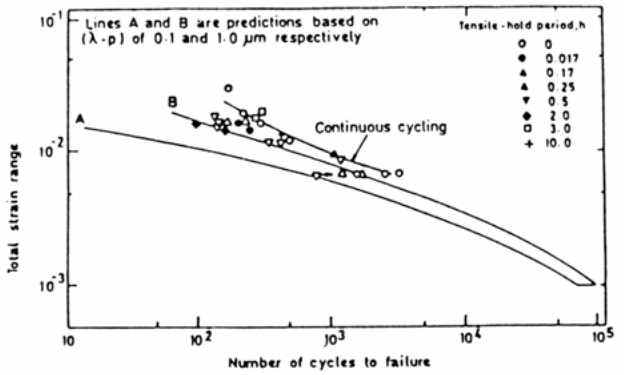

(a) 316 Stainless Steel Cast 58, 625°C (29)

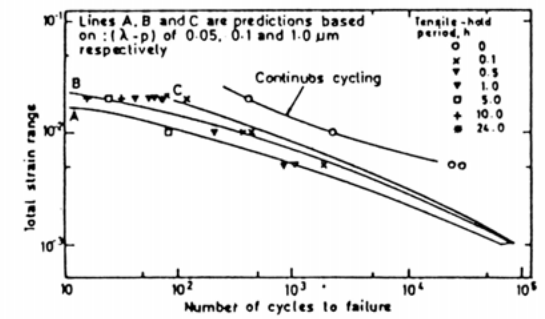

(b) 316 Stainless Steel Cast 65808, 593°C (29)

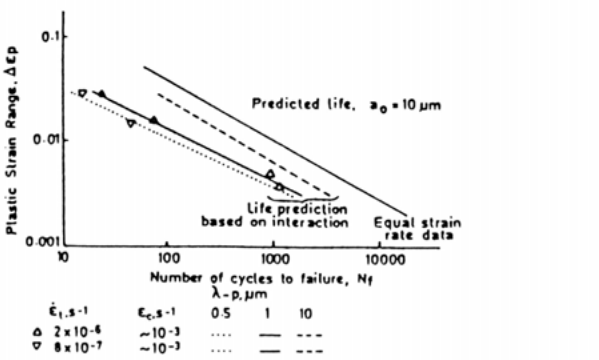

(c) 20% CW & annealed 20/25/Nb Stainless Steel, 593°C (33)

Fig. 31. Interactive crack propagation predictions

stress rupture curves also incorporated in N-47. The total damage D must not go outside the damage envelopes shown in Fig. 33. As noted in Section 3.1, the need for differing values for D, described by the bi-linear line in Fig. 33, reflects the material-dependent uncertainties associated with such an approach.

4.2.2. *Elastic route*

For the elastic route, N_d is obtained through the alternative fatigue curves shown in Fig. 34. These fatigue curves stem from data obtained on 304 stainless steel /119, 120/. In order to extrapolate these data to hold times of up to 100 hrs, constitutive creep relaxation equations were invoked /119/. Using these equations, the creep term $\Sigma(T/T_d')$ was established, and a fatigue life reduction factor evaluated using equation (28). The elastic route fatigue curves (Fig. 34) were obtained by applying the fatigue life reduction factor to the continuous cycle design curves, Fig.. 32. The creep damage term is obtained in a similar way to that described for the inelastic route.

There are thus two routes through which Code Case N-47 can be used. With the inelastic route, conservatism is obtained empirically through factors included with the fatigue curves and through the use of an increased "effective" stress value for obtaining T_d' values in equation (28). With the elastic route, it appears that the creep damage is assessed twice, once through the fatigue curves shown in Fig. 34, which include hold time and slow strain rate effects, and once through the creep damage term $\Sigma(T/T_d')$. These differences in approach reflect uncertainties with the linear life fraction approach and are in addition to those problems outlined in Section 3.1.

A potential improvement to the N-47 Code Case is therefore offered in the next section, along with some suggestions for future work.

4.3. *Future Developments*

It is clear from the foregoing section that there are a number of problems associated with the use of the linear life fraction approach as the basis of design Code Case N-47 /5/. Not least of these is the phenomenological nature of the approach and the generally poor predictions obtained from its application (Section 3.1). However, the problem of finding a better, but equally simple, approach is not easily resolved. Of the many prediction techniques described in Section 3, those found to be most accurate were the damage rate approach (Section 3.4) and ductility exhaustion (Section 3.5). Unfortunately, the damage rate approach is both complicated to apply, and requires numerous material constants, some of them derived from cyclic-hold tests. In contrast, the ductility exhaustion technique is simple to use and, in theory at least, requires only simple fatigue and creep ductility data. Further, it is the method that can most easily be accommodated as a development of N-47 through the straightforward replacement of the creep damage term $\Sigma(T/T_d')$ by $(D_c/\Delta\epsilon_{ct})$ where $\Delta\epsilon_{ct}$ is the tensile creep strain component at half life. However, this raises the question of whether the creep component should be assessed on a time or strain basis. Support for the use of a strain

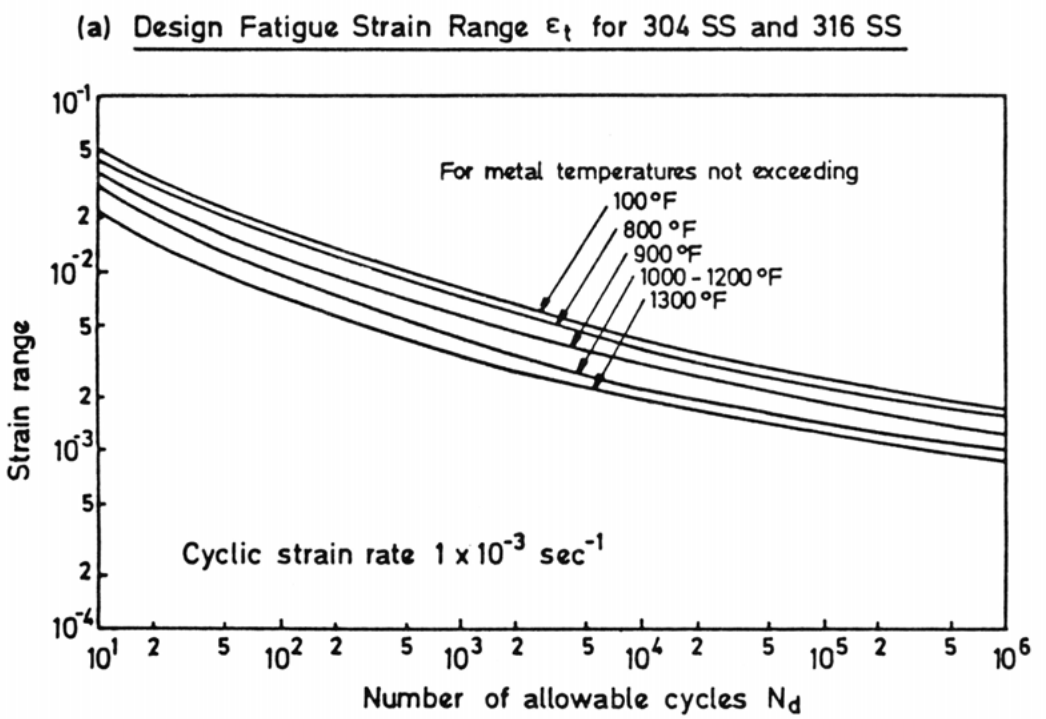

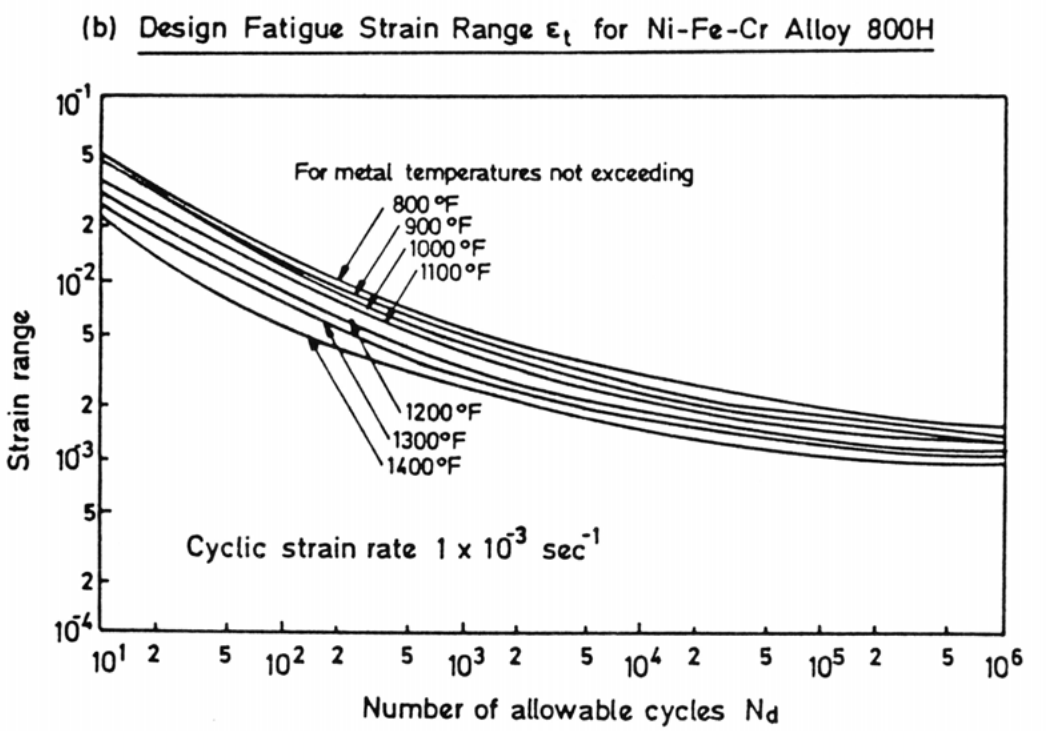

Fig. 32. ASME Code Case N-47 design curves for inelastic route /5/

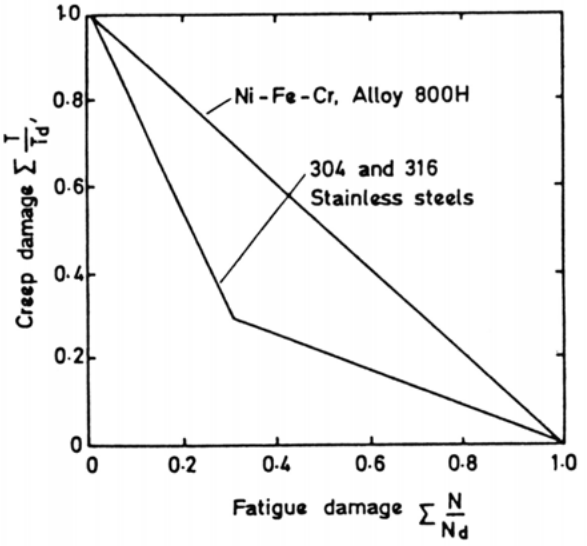

Fig. 33. Linear damage fatigue-creep design envelopes. ASME press. vessel Code Case N-47 /5/

rather than a time fraction basis to assess cyclic creep damage is briefly described below.

Consider two extreme conditions of stress relaxation during constant strain tensile hold periods (Fig. 35). Firstly, taking the case where no relaxation occurs during the hold period, the ductility exhaustion technique would predict no creep damage, since no creep strain would be accumulated. Conversely, a large value for T/T_d' could still be obtained (since at the peak stress, T_d' would be small) and would be used to quantify creep damage even in the absence of any accumulated creep strain. For the situation where extensive relaxation occurs quickly at first, down to a slowly decreasing plateau value, the low relaxed stress attained would imply large values for the rupture time T_d' and therefore small T/T_d' fractions (i.e. relatively non-damaging). However, ductility exhaustion predicts that at the low strain rates exhibited during most of the dwell, with a concomitant low ductility D_c, a relatively larger damaging creep component would in fact exist. Thus the ductility exhaustion approach can be seen to correctly predict the expected relative damaging effects of these two extremes of dwell behaviour, thereby giving support to a strain based prediction approach rather than a time based one. The other main advantage of the ductility exhaustion approach over the time fraction method, is in its mechanistic background /103/. Basically, a given amount of true creep strain $\Delta\epsilon_{ct}$ is accumulated each cycle, (this strain can be directly related to the growth of cavities /103/) and exhausts a fraction of the available ductility of the material. Failure occurs when this ductility is used up, resulting in a given number of cycles to failure equal to $D_c/\Delta\epsilon_{ct}$.

Although it is evident to the authors that the way forward with N-47 is the incorporation of a strain based ductility exhaustion approach, a number of questions still need to be answered:

(1) Which ductility data should be used, particularly in view of the effects of triaxiality and mechanical strain limiting on the value of the transition strain rate, and the effect of service exposure on the ductility?

(2) How do we partition the hold period to determine the true creep strain damage component?

(3) What is the lower limit regarding strain range, beyond which no creep damage will accumulate?

Clearly, to avoid problems associated with identifying the transition strain rates from low to high ductility behaviour, the use of lower bound data must be recommended, even though under certain circumstances this could be overly pessimistic. The only assumption inherent with the ductility exhaustion approach is then that the lower shelf ductilities are themselves independent of triaxial/strain limited testing effects. This could be examined simply by performing tests on notched tensile specimens (to vary the extent of triaxiality) and by observing any degradation in ductility data on the lower shelf.

It should be noted that the use of lower bound ductility data is consistent with the alternative approach used by some workers /107/ of using ductility values derived from the Monkman-Grant relationship,

$$\dot{\epsilon} t_r = \text{const.} \tag{29}$$

where $\dot{\epsilon}$ is the steady state strain rate and t_r the rupture time, instead of from measured ductility values. As shown in Figure 13, this too results in lower ($< 8\%$) ductility values being used.

As far as the partitioning of hold periods into "true" creep and plasticity components, a number of approaches have been forwarded. Priest and Ellison /52/ took advantage of the extensive metallographic data available on their 1CrMoV steel /11/ to estimate transition strain rates between the dominant cavitation mechanisms. This was supported by a more theoretical approach in which a grain boundary sliding regime was included into the deformation mechanism map for 1CrMoV steel, in order to get the critical strain rates at the onset of intergranular damage /101/; this was also achieved for 316 stainless steel /102/. An

(a) Design Fatigue Strain Range ε_t 304 SS and 316 SS-Elastic Analysis

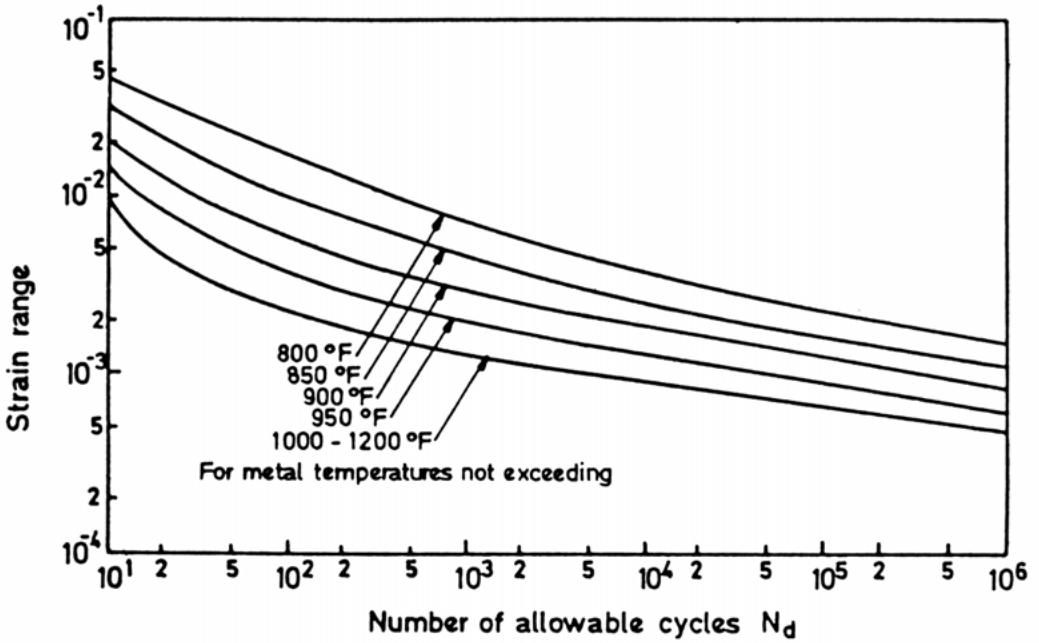

(b) Design Fatigue Strain Range ε_t for Ni-Fe-Cr (Alloy 800H)-Elastic Analysis

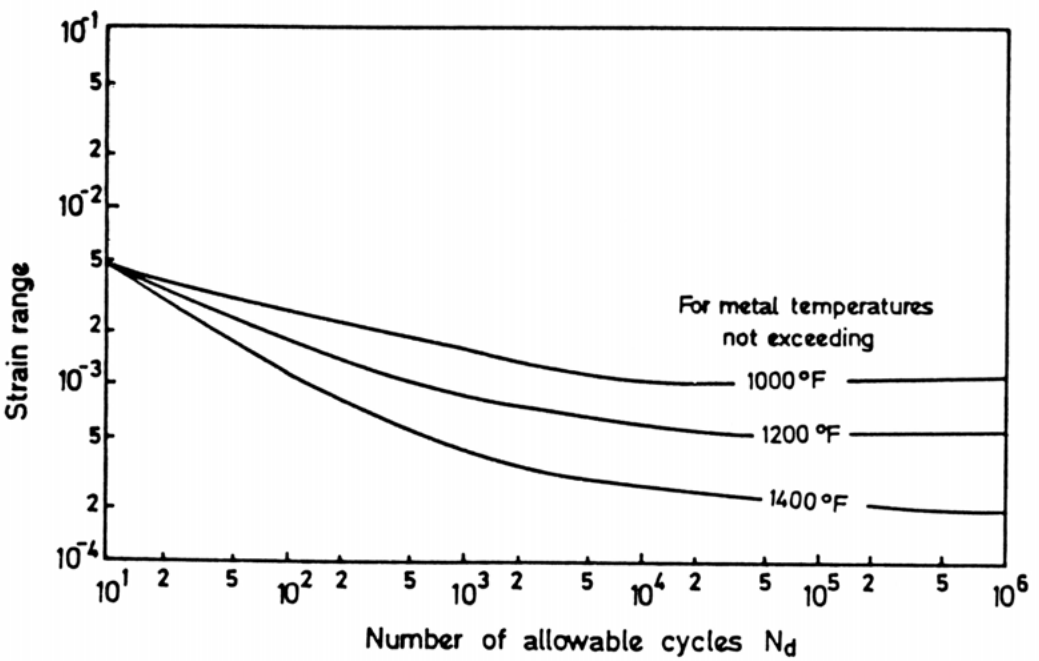

Fig. 34. ASME Code Case N-47 design curves for elastic route /5/

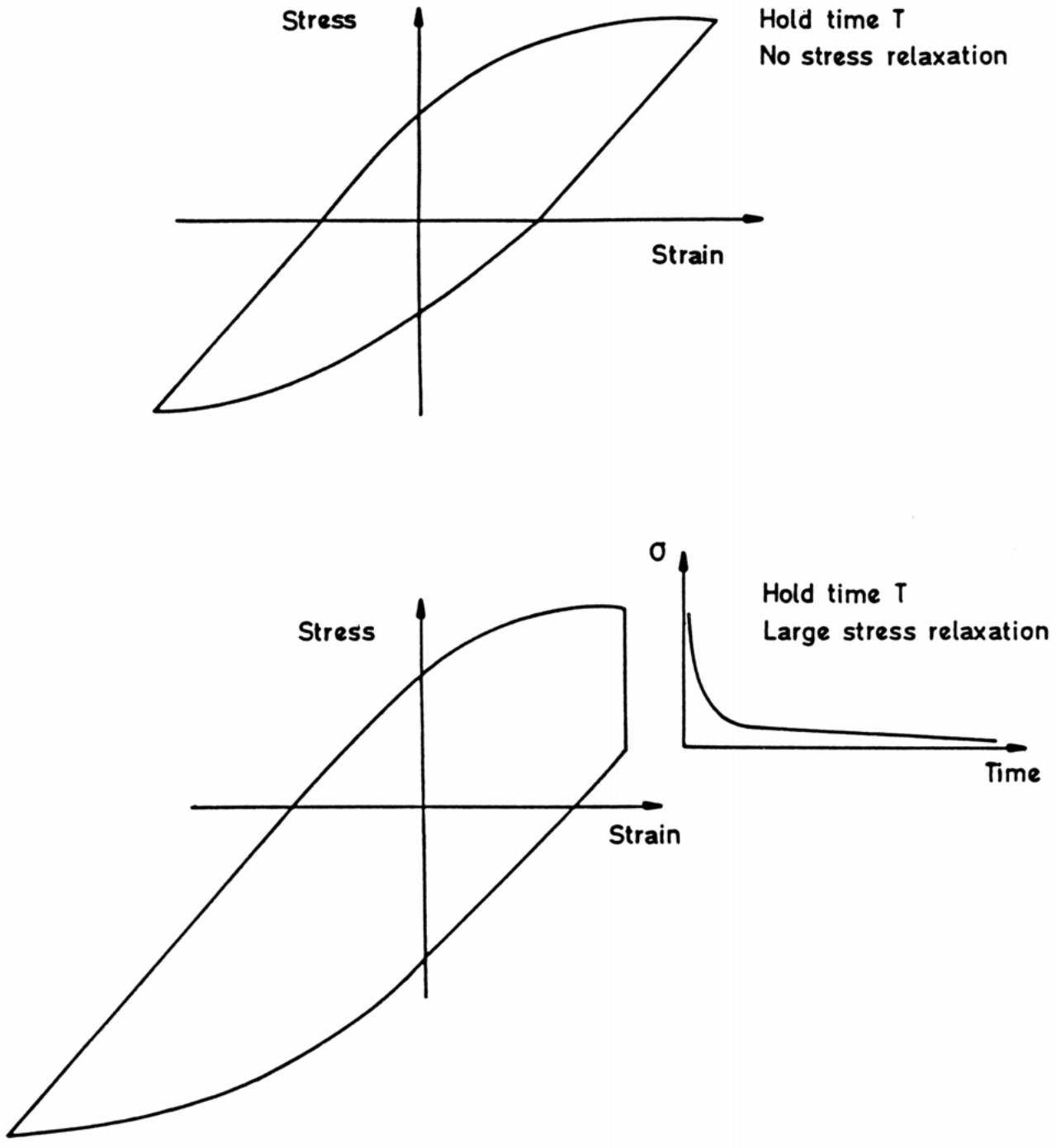

Fig. 35. Schematic extremes of dwell test relaxation behaviour

alternative method for predicting the critical transition strain rates can be found by equating cavity growth rate equations for constrained and unconstrained mechanisms, and solving for the transition strain rate, such that /104/:

$$\dot{\epsilon} = \frac{8\pi D_{gb}\Omega W\sigma B}{kT\lambda^2 d} \qquad (30)$$

where

$$B = [(4\ln\frac{\lambda}{p}) - (1 - (\frac{p}{\lambda})^2)(3 - (\frac{p}{\lambda})^2)]^{-1},$$

D_{gb} is the grain boundary diffusion coefficient, Ω the atomic volume, p the cavity diameter, W the grain boundary width and λ the cavity spacing. However, as with any mechanistic approach there are problems

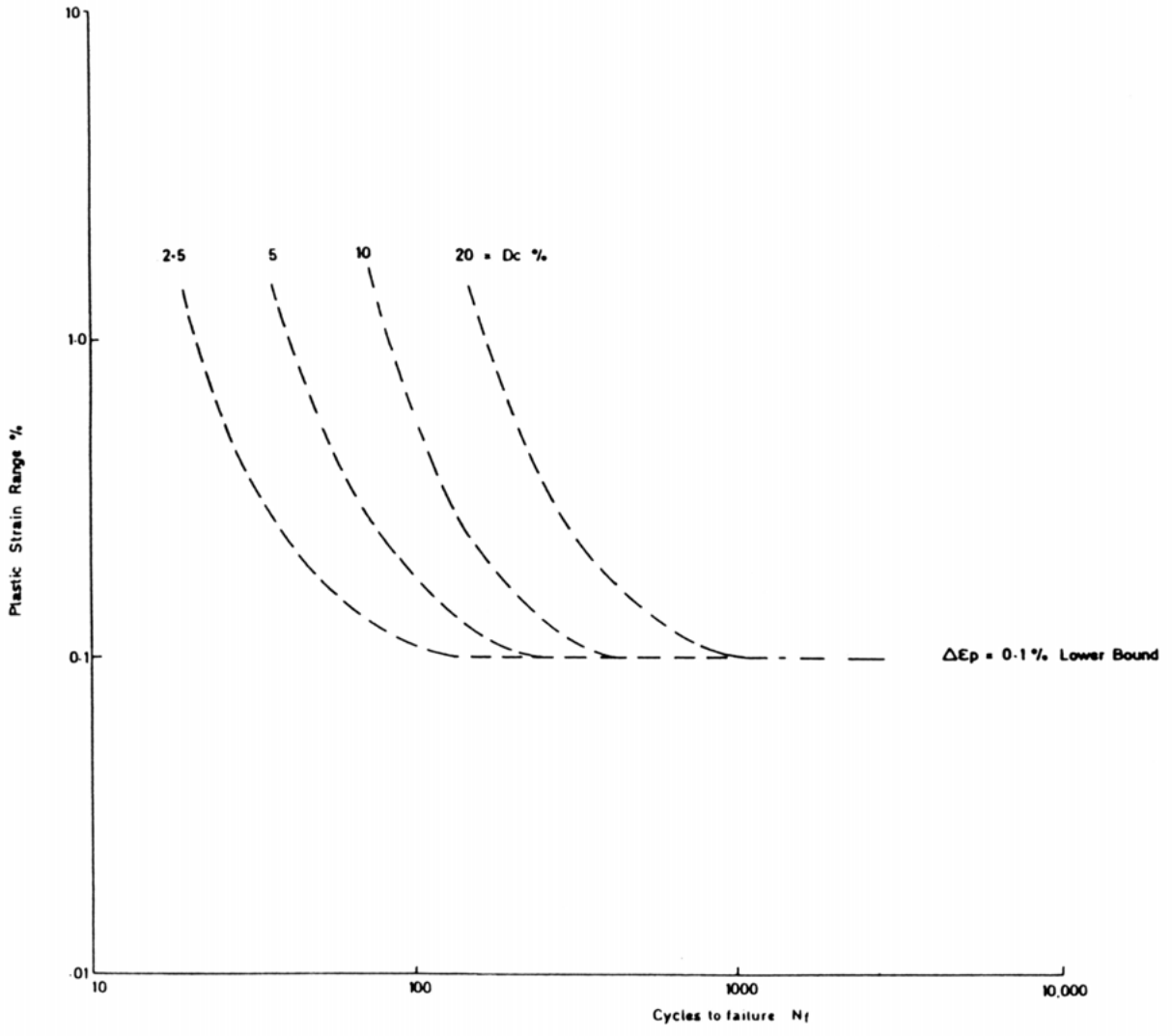

Fig. 36. Effect of creep ductility on endurance predicted from the ductility exhaustion approach

regarding the input data (e.g. the values of λ and D_{gb}). Nevertheless predictions from equation (30), shown in Fig. 13, can be seen to give reasonable agreement with the observed behaviour.

Thus a number of routes are available to obtain transition strain rate values and thereby partition dwell periods into their mechanistically correct subdomains. Although a more robust method of establishing the transition values need to be found, it is clear that the ductility exhaustion method can be incorporated within the N-47 route.

The final point regarding the ductility exhaustion approach is the determination of the limit of this technique at very low strain ranges (i.e. what is the threshold strain range below which no creep damage accumulates). At present no experimental data are available to answer this question. However, it is suggested that a conservative estimate would be the yield strain of the material. This would provide a lower bound for the ductility exhaustion endurance line, as shown in Fig. 36 based on equation (15). Fig. 36 shows various predicted endurance lines for 1Cr-½Mo steel for different values of D_c, the limit to endurance being the yield strain (0.1%).

Taking the above considerations into account, it is clear that the ductility exhaustion method can be used with the N-47 route to yield fundamentally based and potentially more accurate predictions using the equation:

$$\Sigma \frac{N}{N_d} + \frac{D_c}{\Delta \epsilon_{ct}} = 1 \qquad (31)$$

where N_d is the inelastic fatigue life.

The equation evolves from a direction replacement of the creep fraction term in equation (28) with a strain fraction term. However, it is possible that equation (31), should be written as:

$$\Sigma \frac{N}{N_d} \quad \text{or} \quad \frac{D_c}{\Delta \epsilon_{ct}} = 1 \qquad (32)$$

since we have demonstrated throughout this review that the fatigue-creep interaction region occurs over a very narrow band of testing conditions. It follows that failures will generally be either creep or fatigue dominated. In fact the conditions encountered during service will commonly be one of small strain range (less than 0.2%) and long dwell periods, favouring creep dominated failures. Therefore, one clear area for future work is the need to determine which equation, (31) or (32) is most suited for incorporation into N-47.

It is evident that in the past few years the original picture of fatigue-creep, which was based on interaction between a growing fatigue crack and creep damage, has now changed. The initial picture evolved due to tests being conducted at short hold times and high strain ranges on creep-ductile materials. However, recent data on brittle materials, or on long dwell times and small strain ranges, have revealed a failure mode which is creep dominated. It is this mechanism of failure which is likely to predominate under service conditions. Hence previous testing has not been directly relevant to the failure processes encountered at the strain levels relevant to high temperature plant. Indeed it is now becoming clear that the interaction regime is only a narrow zone of behaviour, dividing the fatigue and creep dominated regimes. The global picture of fatigue-creep behaviour is still slowly emerging. It is instructive to examine what progress has been made in identifying the dominant damage regimes under fatigue-creep testing. One useful technique of demonstrating this is to map the failure mechanisms, in a similar way to that of Ashby's creep deformation and fracture maps /8, 9/. A first attempt at mapping fatigue-creep failure mechanism for 1CrMoV, using ductility exhaustion for the creep dominated failure and the simple Manson-Coffin fatigue law for fatigue dominated failures is shown in Fig. 37 /121/. Agreement between observed and predicted behaviour was found to be good. Any interaction failures would lie close to the boundary separating the two failure mechanisms. In addition, these boundary positions will be very dependent on the material's ductility.

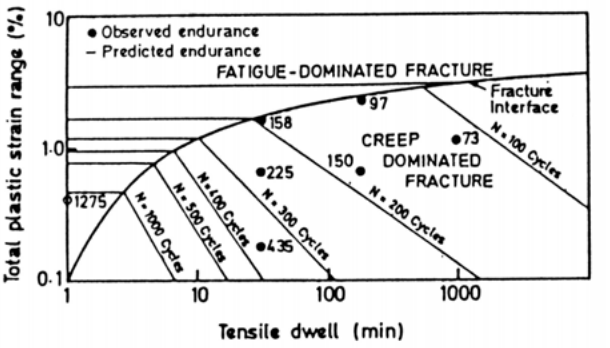

Fig. 37. Fatigue-creep failure mechanism map for 1CrMoV at 565°C /121/

The lower the ductility, the further will the creep dominated region extend.

Figure 37 was based on theoretical equations. A more general qualitative map for the tensile dwell testing of 316 stainless steel has been put forward recently /122/, (Fig. 38). This is a normal plot of endurance data (i.e. $\Delta\epsilon_p$ vs. N_f) which has been subdivided into four regions:

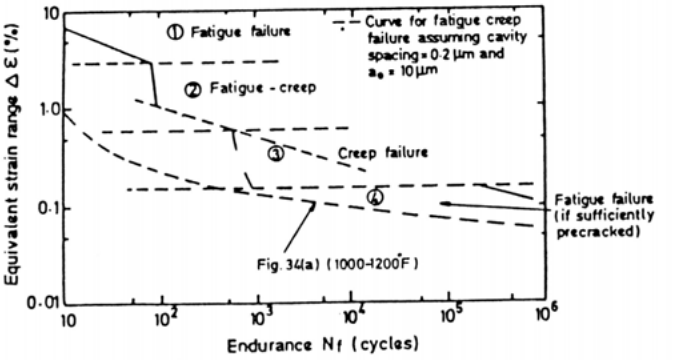

Fig. 38. Composite failure curve under fatigue-creep conditions – type 316 at 600°C /122/

Region (1) at strain range levels $> 3\%$. Failure is fatigue dominated since no creep cavitation has developed.

Region (2) $3\% > \Delta\epsilon > 0.6\%$. Failure is by fatigue-creep interaction.

Region (3) $\Delta\epsilon < 0.6\%$. In this region, failure is creep dominated and results from the accumulation of creep damage. It is favoured by long hold times, small strain ranges and low creep ductility (caused by brittle cast, irradiation, or weldments). It is this region alone where the ductility exhaustion can be applied. A strain range equal to ϵ_y (yield strain) is

eventually reached, below which creep damage does not accumulate.

Region (4) $\Delta\epsilon < \epsilon_y$. Fatigue failure if sufficiently pre-cracked.

In Fig. 38 the area of interest to high temperature plant (i.e. low strain range, long dwell periods) is region (3). The endurance line in Fig. 38 for this region was determined via a ductility exhaustion approach using $D_c = 10\%$. It has already been shown in Fig. 36 how this line moves towards reduced cycles to failure as the ductility decreases. Consequently, applying this concept to Fig. 38 shows that the hold time adjusted fatigue damage line (Fig. 34) from N-47, which is superimposed on Fig. 38 could be transgressed. It is therefore this region that should be examined closely through future test programmes, together with confirmation that the constitutive equations used to predict relaxation behaviour during long hold times are indeed representative. Finally, Fig. 38 shows the importance of the ductility parameter, and illustrates the detrimental consequence, in terms of endurance, of reducing ductility due to metallurgical changes caused by irradiation, ageing, etc.

This review has considered fatigue-creep behaviour primarily under uniaxial loading, however many components operating in high temperature plant are subject to multiaxial deformation. At present, data on the fatigue-creep behaviour of engineering alloys under multiaxial deformation conditions is limited, consequently this area has not been covered in the review. Nevertheless, it is an important area which needs to be investigated in the future. In particular, the application of the ductility exhaustion approach, based on strain summation, to multiaxial deformation needs to be addressed. (i.e., is it maximum principal strain or equivalent strain that has to be considered?).

5. CONCLUDING REMARKS

This review has attempted to examine general trends in materials response due to fatigue-creep loading conditions. Existing life prediction techniques have been reviewed, and the most viable highlighted and assessed against a range of test data. The importance of ductility in determining the life and failure modes of ferritic and stainless steels under fatigue-creep conditions has been noted. Indeed, it has been shown that when failures are creep dominated, a ductility exhaustion approach to life prediction seems to be the best currently available. In particular, the primary advantage of this method is that it takes account of the known effect of service exposure on the ductility of engineering materials. However, it has been shown that the area of fatigue-creep interaction still requires further modelling in order to produce a similarly accurate and simple life prediction technique.

At present, the only available code for designing against fatigue-creep conditions is the ASME Code Case N-47. The advantages and disadvantages of this code have therefore been examined. It is proposed that the introduction of a strain based ductility exhaustion term, in place of the existing time based creep term, into the N-47 route should provide the most suitable improvement on the code. Mechanistically-based arguments have been forwarded to support this proposal. However, before such amendments can be made to N-47, a number of points have to be resolved. These form the basis of future work recommendations:

(1) Data sheets are required which list ductility values as a function of strain rate for a range of engineering materials.

(2) An examination of the effect of strain limited deformations on ductility data, especially the lower bound values, is needed.

(3) An investigation into whether the fatigue and creep damage terms in the life equations are independent or additive must be made.

(4) The influence of multiaxial deformation on fatigue-creep behaviour and its incorporation into the ductility exhaustion approach needs to be examined.

(5) Reliable constitutive equations which can be used to obtain stress relaxation data and the peak stress in a fatigue cycle, need to be produced.

REFERENCES

1. BEAUCHAMP, D.J. and ELLISON, E.G., *J. Strain Anal.*, **17**: 1, 45–52 (1982).
2. KUWABARA, K., NITTA, A. and KITAMURA, T., *Advances in Life Prediction*, ed. by D.A. Woodford and J.R. Whitehead, 131–142, ASME (1983).
3. COFFIN, L.F., *Proc. I. Mech. E.*, **188**: 19/74 (1974).
4. ELLISON, E.G. and HARPER, M.P., *J. Strain Anal.*, **13**: 1, 35–51 (1978).
5. ASME Boiler and Press. Vess. Code, Section III, CODE CASE N-47 (1974).
6. PLUMBRIDGE, W.J. and MILLER, K.J., *Creep Strength in Steels and High Temperature Alloys*, Iron and Steel Inst., 50 (1972).
7. HALES, R., *Fat. Engng. Mater. Struct.*, **3**: 339 (1980).
8. ASHBY, M.F., *Acta Met.*, **20**: 887–897 (1972).

9. ASHBY, M.F., GANDHI, C. and TAPLIN, D.M.R., *Acta Met.*, **29**: 699–729 (1979).
10. ELLISON, E.G. and PATERSON, A.J.F., *Proc. I. Mech. E.*, **190**: 12/76, 321–350 (1976).
11. PLUMBRIDGE, W.J., PRIEST, R.H. and ELLISON, E.G., *Proc. ICM3*, **2**: 129 (1979).
12. BATTE, A.D., MURPHY, M.C. and STRINGER, M.B., *Met. Tech.*, **5**: 12, 405–413 (1978).
13. MELTON, K., *Mat. Sci. Eng.*, **55**: 21–28 (1982).
14. BRINKMAN, C.R., STRIZAK, J.P. and BROOKER, M.K., AGARD Conf. Proc. 243 (1978).
15. MILLER, D.A. and GLADWIN, D., to be published.
16. DAWSON, R.A.T., ELDER, W.J., HILL, G.J. and PRICE, A.T., *Thermal and High Strain Fatigue*, Metals and Metallurgy Trust, Mono 32, 23 (1967).
17. WOOD, D.S., BALDWIN, A.B. and WILLIAMSON, K., UKAEA Report ND-R-253(R) (1979).
18. CHALLENGER, K.D., MILLER, A.K. and BRINKMAN, C.F., *J. Eng. Mat. and Tech.*, **103**: 7 (1981).
19. EDMUNDS, H.G. and WHITE, D.J., *J. Mech. Eng. Sci.*, **8**: 3, 310–321 (1966).
20. WAREING, J., *Met. Trans.*, **8A**: 711–721 (1977).
21. BRINKMAN, C.R., KORTH G.E. and HOBBINS, R.R., *Nuc. Tech.*, **16**: 299–307 (1972).
22. CONWAY, J.B., BERLING, J.T. and STENTZ, R.H., GEC Note GEMP-740 (1969).
23. ASADA, Y. and MITSUHASKI, S., *4th Int. Conf. Press. Vess. Tech.*, **1**: 321 (1980).
24. BRINKMAN, C.R. and KORTH, G.E., *Met. Trans.*, **5**: 792 (1974).
25. WAREING, J., *Met. Trans.*, **6A**: 1367 (1975).
26. WAREING, J., VAUGHAN, H.G. and TOMKINS, B., UKAEA Rep. ND-R-447(S) (1980).
27. GOODALL, I.W., HALES, R. and WALTERS, D.J., Proc. IUTAM, 103 (1980).
28. WOOD, D.S., WYNN, J., BALDWIN, A.B. and O'RIORDAN, P., *Fat. of Eng. Mat. and Struct.*, **3**: 89 (1980).
29. WAREING, J., *Fat. of Eng. Mat. and Struct.*, **4**: 131 (1981).
30. LAI, J.K. and HORTON, C.P., CEGB Rep. RD/L/R/2008 (1979).
31. HALES, R., Int. Conf. on Creep and Fract. of Eng. Mat., Swansea (1984).
32. MAJUMDAR, S. and MAIYA, P.S., *J. Eng. Mat. and Technol.*, **102**: 1, 159 (1980).
33. LIVESEY, V.B. and WAREING, J., *Met. Sci.*, **17**: 297 (1983).
34. GLADWIN, D. and MILLER, D.A., *Fat. of Eng. Mat. and Struct.*, **5**: 275–286 (1982).
35. GLADWIN, D. and MILLER, D.A., to be published.
36. OSTERGREN, W.J., *J. Test. and Eval.*, **4**: 327–339 (1976).
37. HYZAK, J.M. and BERNSTEIN, H.L., AGARD Conf. Proc. 243 (1978).
38. ANTUNES, V.T.A. and HANCOCK, P., *ibid.*
39. LORD, D.C. and COFFIN, L.F., *Met. Trans.*, **4**: 1647–1653 (1973).
40. KORTOVICH, C.S. and SHEINKER, A.H., AGARD Conf. Proc. 243 (1978).
41. WELLS, C.H. and SULLIVAN, C.P., *ASM, Trans. Quart.*, **60**: 217–222 (1967).
42. WELLS, C.H. and SULLIVAN, C.P., ASTM STP 459, p. 59 (1968).
43. SIKKA, V.K., ORNL Rep. ORNL/TM-6608 (1978).
44. HALES, R. and CORDWELL, J.E., private communication (1982).
45. HALES, R., CEGB Report TPRD/B/0288/N/83 (1983).
46. BEECH, S.M. and BATTE, A.D., Int. Conf. on Creep and Fract. of Eng. Mat., Swansea, 1043–1054 (1984).
47. POWELL, D.J., PILKINGTON, R. and MILLER, D.A., *ibid.*
48. HANCOCK, J.W., *Met. Sci.*, **10**: 319 (1976).
49. SPEIGHT, M.V. and HARRIS, J.E., *Met. Sci.*, **1**: 83 (1967).
50. SPEIGHT, M.V. and BEERE, W., *Met. Sci.*, **9**: 190 (1975).
51. DYSON, B.F., *Can. Met. Quart.*, **18**: 31 (1979).
52. PRIEST, R.H. and ELLISON, E.G., *Int. Conf. Eng. Aspects of Creep*, **1**: 185–192 (1980).
53. DYSON, B.F. and LOVEDAY, M.S., Proc. 3rd IUTAM Conf., 408 (1980).
54. COFFIN, L.F., ASTM STP 520, 5 (1973).
55. WHITE, D.J., *Proc. I Mech. E.*, **164**: 223 (1969).
56. SOLOMON, H.D. and COFFIN, L.F., ASTM STP 520, 112 (1973).
57. WOOD, D.S., SLATTERY, G.F., WYNN, J., CONNAUGHTON, M.D. and LAMBERT, M.E., Proc. Conf. Inf. of Env. on Fatig., I Mech. E., 11–20 (1977).
58. LEVAILLANT, C., REZQUI, B. and PINEAU, A., *Proc. ICM3*, **2**: 163–172 (1979).
59. JASKE, C.E. and RICE, R.C., ASME MPC-3, 101 (1976).
60. MARSHALL, P., Proc. Conf. Inf. on Env. on Fatigue, I Mech. E. (1977).
61. HARROD, D.L. and MANJOINE, M.J., ASME MPC-3, p. 87 (1976).
62. GELL, M. and LEVERANT, G.R., ASTM STP 520, 37 (1973).
63. SCARLIN, R.D., *Proc. ICF4*, **2**: 849 (1977).
64. HAIGH, J.R., SKELTON, R.P. and RICHARDS, C.E., *J. Mat. Sci. and Eng.*, **26**: 167 (1976).
65. TOMKINS, B., UKAEA Rep. ND-R-415 (s) (1980).
66. KACHANOV, L.M., *Advances in Creep Design*, App. Sci. Publ. Ltd. (1971).
67. LEMAITRE, J. and CHABOCHE, J.L., Proc. IUTAM (1974).
68. CHRZANOWSKI, M., *Int. J. Mech. Sci.*, **18**: 69–73 (1976).
69. PLUMTREE, A. and LEMAITRE, J., Proc. ICF5, 2379 (1981).

70. PRIEST, R.H. and ELLISON, E.G., *Res Mech.*, **4**: 127–150 (1982).
71. MINER, M.A., *J. Appl. Mech.*, **12**: 3, A159–A167 (1945).
72. ROBINSON, E.L., *Trans. ASME*, **74**: 5, 777–781 (1952).
73. TAIRA, S., *Creep in Structures*, Acad. Press, 96–124 (1962).
74. JASKE, C.E., MINDLIN, H. and PERRIN, J.S., ASTM STP 520, 365 (1973).
75. MAIYA, P.S., Argonne Nat. Lab. Rep. ANL-78-59 (1978).
76. CAMPBELL, R.D. and VELJOVICH, W., Proc. SMIRT4 (1977).
77. COFFIN, L.F., ASME MPC-3, 349 (1976).
78. MAJUMDAR, S. and MAIYA, P.S., *Can. Met. Quart.*, **18**: 57–64 (1979).
79. OSTERGREN, W.J., ASME MPC-3, 179 (1976).
80. MANSON, S.S., ASTM STP 520, 744–782 (1973).
81. MANSON, S.S., HALFORD, G.R. and HIRSCHBERG, M.H., NASA Report TMX-67838 (1971).
82. HALFORD, G.R., HIRSCHBERG, M.H. and MANSON, S.S., ASTM STP 520, 658 (1973).
83. HALFORD, G.R., SALTSMAN, J.F. and HIRSCHBERG, M.H., NASA Tech. Note TM-73737 (1977).
84. HALFORD, G.R. and MANSON, S.S., ASTM STP 612, 239 (1976).
85. MANSON, S.S., HALFORD, G.R. and NACHTIGALL, A.C., *Adv. in Design for Elev. Temp. Env.*, ASME Nat. Congr. Press.Vess. and Piping, 17 (1975).
86. PARRUCHET, C., AGARD Conf. Proc. 243 (1978).
87. GREENSTREET, W.L., *Nuc. Eng. and Design*, **50**: 411–424 (1978).
88. ELLISON, E.G., BEAUCHAMP, D.J. and PRIEST, R.H., University of Bristol Report 78/3 (1978). Also in AGARD Conf. Proc. 243 (1978).
89. MANSON, S.S. and HALFORD, G.R., ASME MPC-3, 299 (1976).
90. ZAMRIK, S.Y., AGARD Conf. Proc. 243 (1978).
91. HALFORD, G.R. and SALTSMAN, J.F., ASME Conf. "Advances in Life Prediction Methods", 17–26 (1983).
92. SALTSMAN, J.F. and HALFORD, G.R., NASA Tech. Note TMX-71898 (1976).
93. SALTSMAN, J.F. and HALFORD, G.R., NASA Tech. Note TMX-73474 (1976).
94. CHABOCHE, J.L., POLICELLA, H. and KAEZMAREK, H., AGARD Conf. Proc. 243 (1978).
95. KUBARA, K.K. and NITTA, A., *Proc. ICM3*, **2**: (1979).
96. DAY, M.F. and THOMAS, G.B., AGARD Conf. Proc. 243 (1978).
97. MAJUMDAR, S. and MAIYA, P.S., ASME MPC-3, 323 (1976).
98. MAJUMDAR, S. and MAIYA, P.S., Proc. ICM2, 924–928 (1976); Also Argonne Nat. Lab. Report ANL-76-58 (1976).
99. MAJUMDAR, S. and MAIYA, P.S., ASME-CSME Press. Vess. and Piping Conf., PVP-PB-028 (1978).
100. MAJUMDAR, S. and MAIYA, P.S., *Proc. ICM3*, **2**: 101–109 (1979).
101. PRIEST, R.H. and ELLISON, E.G., *Mat. Sci. and Eng.*, **49**: 7 (1981).
102. PRIEST, R.H., BEAUCHAMP, D.J. and ELLISON, E.G., ASME Conf. "Advances in Life Prediction Methods", 115–122 (1983).
103. MILLER, D.A., HAMM, C.D. and PHILLIPS, J.L., *Mat. Sci. and Eng.*, **53**: 233–244 (1982).
104. DYSON, B.F. and LOVEDAY, M.F., *Proc. Int. Conf. on Engng. Aspects of Creep*, **1**: 61 (1980).
105. MILLER, D.A., ASME Conf. "Advances in Life Prediction Methods", 157–163 (1983).
106. BEERE, W., to be published in *Voids, Cavities and Cracks in Metallic Alloys*, ed. J.H. Gittus, Appl. Sci., New York (1984).
107. HALES, R., *Fat. Energ. Mater. Struct.*, **6**: 121 (1983), and also CEGB Report TPRD/B/0038/N82 (1982).
108. TOMKINS, B., *Phil. Mag.*, **18**: 1041–1066 (1968).
109. TOMKINS, B., UKAEA Report TRG 2686(S) (1975).
110. WAREING, J., TOMKINS, B. and SUMNER, G., ASTM STP 520, 123 (1973).
111. TOMKINS, B. and WAREING, J., Proc. Int. Conf. on Corrosion Fatigue, NACE-2, 303–311 (1972).
112. CHENG, C.F. and CHENG, C.V., Argonne Nat. Lab. Rep. ANL-8002 (1974).
113. TOMKINS, B. and WAREING, J., *Met. Sci.*, **11**: 414 (1977).
114. WAREING, J. and TUREK, M., unpublished results, NPDL (1981).
115. LLOYD, G.J. and WAREING, J., *J. Eng. Mat. Tech. (Trans. ASME)*, **101**: 275 (1979).
116. MICHEL, D.J. and SMITH, H.H., *Acta Met.*, **28**: 999–1007 (1980).
117. MARSHALL, P. and BRINKMAN, C.R., ASME MPC-15, 15–32 (1980).
118. JAMES, L.A., *Int. J. Frac. Mech.*, **8**: 347 (1972).
119. CONWAY, J.B., GEC Note GEMP-730 (1969).
120. BERLING, J.T. and CONWAY, J.B., Proc. First Int. Conf. on Press. Vess. Tech., Delft (1969).
121. MILLER, D.A., *Mat. Sci. Eng.*, **54**: 273 (1982).
122. TOMKINS, B. and HALES, R., ASME 82-PVP-70 (1982).